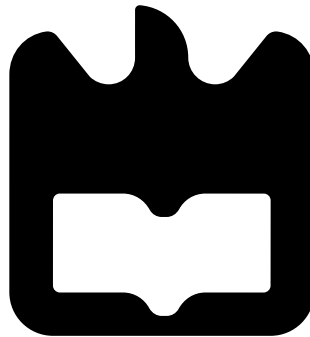**André
Correia de Costa
Barros**

**Propagação de sinais de rádio sobre fibra no
contexto de NG-PON2**

**Propagation of radio over fiber signals on the
context of NG-PON2**

**André
Correia de Costa
Barros**

Propagação de sinais de rádio sobre fibra no contexto de NG-PON2

Dedico este trabalho aos meus pais, à minha irmã e ao meu irmão.

O júri

Presidente

Professor Doutor Paulo Miguel Nepomuceno Pereira Monteiro
Professor Associado da Universidade de Aveiro

Vogais

Professor Doutor Mário José Neves de Lima
Professor Auxiliar da Universidade de Aveiro (Orientador)

Professor Doutor Henrique Manuel de Castro Faria Salgado
Professor Auxiliar da Universidade do Porto

agradecimentos

Primeiramente não poderia deixar de agradecer a mim mesmo, por todas as horas de trabalho que coloquei na execução da tese.

Em seguida, aos meus pais, que foram sem dúvida as pessoas que mais me influenciaram a tentar ser o melhor possível todos os dias e motivaram-me bastante nesta etapa.

À minha irmã por ser fantástica como é e por me motivar sempre a trabalhar e em ir para casa, nem que fosse para trabalhar na mesma.

Ao meu irmão por ser o meu melhor amigo e que sem ele nada seria o mesmo.

Aos Professores Mário Lima e António Teixeira, que me orientaram ao longo deste último ano, um obrigado pelo autonomia e confiança que depositaram em mim.

Ao Ali Shapari, por toda a ajuda na integração inicial ao laboratório que permitiu-me ambientar facilmente.

Ao Ricardo Ferreira, porque apesar de não estar associado em papel ao dsenvolvimento da minha tese sempre ajudou-me com as inúmeras dúvidas que eu tive ao longo da tese e com as melhores soluções para implementar o que era pretendido.

Esta longa etapa também não teria sido a mesma sem os meus colegas de sala, André Almeida, Carla Rodrigues, Sérgio Dias e Tiago Morgado, pois com vocês os dias passados na "despensa" foram melhores.

Em especial ao Tiago Morgado, por estes últimos meses onde fomos autênticos companheiros de batalha para conseguir entregar a tese na data definida.

Sérgio Dias também destacado pela ajuda que deu quando eu precisava de tirar os últimos resultados no laboratório e ele disse-me que tinha que aparecer nos agradecimentos e por isso aqui está a tua menção.

Ao batalhão noturno do laboratório de redes, principalmente ao Rúben e ao Francisco, que me acolheram no laboratório de redes tantas noites e onde me senti sempre em boa companhia.

Uma outra pessoa muito especial que não poderia deixar de aparecer, Rita António por toda a ajuda incondicional que me deu, que me ajudou muito nesta etapa da minha vida.

E em último a todos os meus amigos que fizeram com que tanto este último ano, como todos os outros da universidade tenham sido repletos de bons momentos.

Resumo

Hoje em dia todas os pessoas estão ligadas em rede, e devido à proliferação de diversos serviços torna-se cada vez mais imprescindível arranjar novas opções para fornecer a maior largura de banda possível, para responder às necessidade geradas. As redes óticas passivas de próxima geração surgem como a solução fornecendo ritmos de transmissão na ordem dos Terabits/s e um alcance na ordem dos milhares de kilometros. Neste contexto será falado dos sinais de rádio na fibra, que trazem vantagens ao nível da simplificação das estações base, possibilitando poupança nos custos, isto ao integrar a tecnologia de rádio com a tecnologia de fibra existente

Neste trabalho iniciou-se pelo estudo da literatura existente das arquitectura existentes de radio-sobre-fibra, bem como as suas limitações. De seguida, procedeu-se ao desenvolvimento de uma plataforma de simulação para estudar os fenómenos que o sinal de rádio sofre ao ser transportado no sistema ótico. Por último, foram realizadas experiências laboratoriais, primeiro com um transceiver NG-PON2 e depois com um sistema rádio-sobre-fibra, consistindo o objectivo em caracterizar estes sistemas.

Abstract

Nowadays all the people are connected on a network, and due to the proliferation of several services it becomes indispensable to find new option to provide as more bandwidth as possible to answer to necessity. The next generation passive optical networks rise as a solution to supply transmission rate on the Terabits/s order and a reach on the order of the thousands kilometers. On this context, the radio-over-fiber signals are going to be spoken about, which offer advantages by the simplification of base stations, allowing lower costs, and this by composing the radio technology with the already existent fiber technology.

This work initiated by the study of the existent literature of the radio-over-fiber architectures, as well as their limitations. Then, proceeded on the development of a simulation platform to study the phenomenons that a radio-over-fiber suffers while going through the optical system. For last, laboratory experiments were carried out first with a NG-PON2 transceiver and then with a radio-over-fiber system, being the objective of characterizing these systems.

Contents

List of Figures

List of Tables

Acronyms

ADC Analogue-to-Digital

APD Avalanche Photodiode

ASE Amplified Sponaneous Emission

AWG Arbitrary Waveform Generator

B2B Back-to-Back

BB Baseband

BER Bit Error Rate

BOSA Bidirectional Optical Subassembly

BS Base Station

CO Central Office

CPRI Common Public Radio Interface

CU Central Unit

CW Continuous Wave

D2D Device-to-Device

DAC Digital-to-Analogue

DBR Distributed Bragg Reflector

DFB Distributed Feedback Laser

D-MIMO Distributed Multiple Input-Output

DR Dynamic Range

DRoF Digital Radio-over-Fiber

DSB Dual Sideband

DUT Device Under Test

EAM Electro-Absorption Modulator

EPON Ethernet passive optical network

ER Extinction Ratio

EVM Error Vector Magnitude

FP Fabry-Perot

HDTV High Definition Television

IEEE Institute of Electrical and Electronics Engineers

IF Intermediate Frequency

IM Intermodulation Product

IMD Intermodulation Distortion

IM-DD Intensity Modulation/Direct-Detection

IP Internet Protocol

ITU-T Internation Telecomunication Union - Telecomunication

LASER Light Amplification by Stimulated Emission of Radiation

LO Local Oscillator

LTE Long-Term Evolution

MIMO Multiple-Input-Multiple-Output

mmWave Milimeter Wave

MU Mobile Unit

MZM Mach-Zenhder Modulator

NG-PON2 Next Generation Passive Optical Network Phase 2

NRZ Non-Return-to-Zero

NLSE Non-Linear Schrodinger Equation

OBSAI Open Base Station Architecture

OLT Optical Line Terminal

ONU Optical Network Unit

PSK Phase Shift Keying

PON Passive Optical Network

PtP Point-to-Point

QAM Quadrature Amplitude Modulation

QPSK Quadrature Phase Shift Keying

RAU Remote Antenna Unit

RF Radio Frequency

RFoF RF-over-fiber

RIN Relative Intensity Noise

RMS Root Mean Square

RoF Radio-over-Fiber

ROSA Receiver Optical Subassembly

RRH Remote Radio Head

RSOA Reflective SemiConductor Optical Amplifier

SNR Signal-to-Noise Ratio

SSB Single Sideband

SSFM Split-Step Fourier Method

SSMF Standard Single Mode Fiber

TDM Time Division Multiplexed

TOI Third-Order Intercept

TOSA Transmitter Optical Subassembly

TWDM Time Wavelength Division Multiplexing

UE User Equipment

UHDV Ultra-High Definition Video

USB Universal Serial Bus

VCSEL Vertical Cavity Surface-Emitting Laser

WDM Wavelength Division Multiplexing

x

Chapter 1

Introduction

1.1 Context and Motivation

The delivery of broadband connections has been traditionally targeted by the employment of optical fiber, which has allowed the increase of the provided bandwidth by the diverse telecommunication operators and has resulted on the gradual forgetfulness of the technologies based on copper lines.

However since 2002, the impact of wireless technologies started to be noticeable, as it allowed the end user to a new sensation of freedom, since no physical connection was required but the provision of the required high bit rates, to satisfy the current necessities of the end users, has proven to be a lot harder to achieve wirelessly on contrast with the use of fixed optical communications [1].

In order to implement it, it has been more and less agreed, that the best option consists on using multiple input-output (MIMO) technologies based on multiple antennas at the transceivers in order to exploit the scattering properties of the wireless medium. The problem with this technology is that even though the multiplexing gain theoretically would be given by the minimum number of the receiving/transmitting antennas, if the channel is richly scatter, that rarely ends being the case in an outdoor environment, and therefore the multiplexing gain ends being a lot lower than it's theoretical value. Its also required to take into consideration the interference that will happen if another MIMO users exists, which implies the necessity of joint processing. The number of channels per transceiver is also limited, because of the inherent physical limitation on size of these devices, since the spacing between the antennas becomes more limited and therefore less are allowed to cohabit on the same transceiver. There is also the fact that comparing the MIMO with fully uncorrelated channels, the gain is a lot lower, since there exists and high correlation between channels specially on outdoor environment.

Due to this, a concept was created around the use of distributed MIMO (D-MIMO), in which specific stations could act as antenna elements of a virtual array. The most used implementation of this concept consists on an architecture where the mobiles communicate with several remote antenna units (RAU) that cooperate with each other and correspond to physical distributed antennas of a specific base station, that is known as central unit (CU),

that is responsible for performing all signal processing. This allows for cost saving as the RAU can be greatly simplified, since their purpose on this implementation resides only on performing optoelectronic conversion, filtering and amplification processes.
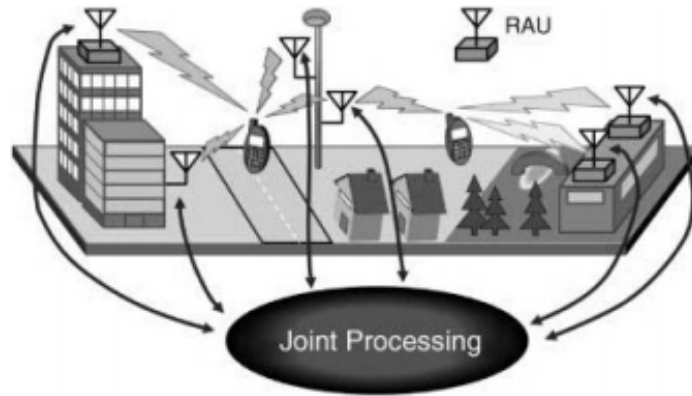
Figure 1.1: Processing of signals from multiples RAUs [1]

1.2 Objectives

With the context and motivation of this work already presented it is time to address the objectives of the dissertation. Due to the increasing development on the optical domain, the operators took the opportunity of growing their radio signals distribution network and due to that the solution of transmitting radio-over-fiber arose. Therefore the main scope of the dissertation is to study and posteriorly analyse the performance of RoF system, and to do so the dissertation had the following objectives:

- Study the NG-PON2 norm.

- Study the RoF system.

- Simulation of a RoF system.

- Laboratory work with a RoF system.

1.3 Structure of the document

The structure of the dissertation is the following:

- **Chapter 2: Radio over Fiber Systems and NG-PON2**
  On this chapter, we start by addressing the NG-PON2 norm and the BOSA transceivers that are used on the OLT/ONU. NG-PON2 consists nowadays on the fundamental of Passive Optical Networks and therefore its study is of importance to the framework of RoF systems, which will be profoundly studied on this chapter.

- **Chapter 3: Simulation of Radio over Fiber System:**
  Allied with the Matlab software a platform is developed with the objective of simulating the steps of generating RoF signals, propagating them through the optical system and

retrieve them to analyse their performance. The platform was also optimized to assist with the experimental work.

After the implementation, several experiments are done which will give a first introduction to the performance of the RoF system, for situation with varying modulation format, fiber length, signal-to-noise ratio and parameters from the signal itself, as the carrier frequency.

- **Chapter 4: Practical Experiment**
  This section of the system is devoted to present the several laboratory experiments performed. The first study was oriented to the BOSA transceivers, followed by the analysis of a RoF system.

- **Chapter 5: Conclusions and Future Work**
  On this section it is discussed the results obtained on the dissertation and a suggestion regarding the work that should be done next on this topic.

Chapter 2

Radio over Fiber Systems and NG-PON2

2.1   NG-PON2

Due to the incessant increase in data consumption, optical fiber access systems based on passive optical networks (*PON*) are currently being deployed by network operators worldwide on a massive market scale. Different Gigabit-class PON systems, such as **G-PON!** and EPON, have already been standardized by the ITU-T and IEEE. The next step in the evolution of fiber access was defined by the ITU-T and it's denominated of NG-PON2. NG-PON2 is a 40Gbits/s capacity PON system that is able of exploiting both the time and wavelength domains. There existed several technologies options that could meet the NG-PON2 standards, but between all of them, the TWDM ended becoming the primary solution, as it was the option the most compatible with the high volume residential application. The aggregated downstream capacity is of 40 Gbit/s and 10 Gbit/s upstream, since 4 channels are used respectively with 10 Gbit/s and 2.5 Gbit/s.
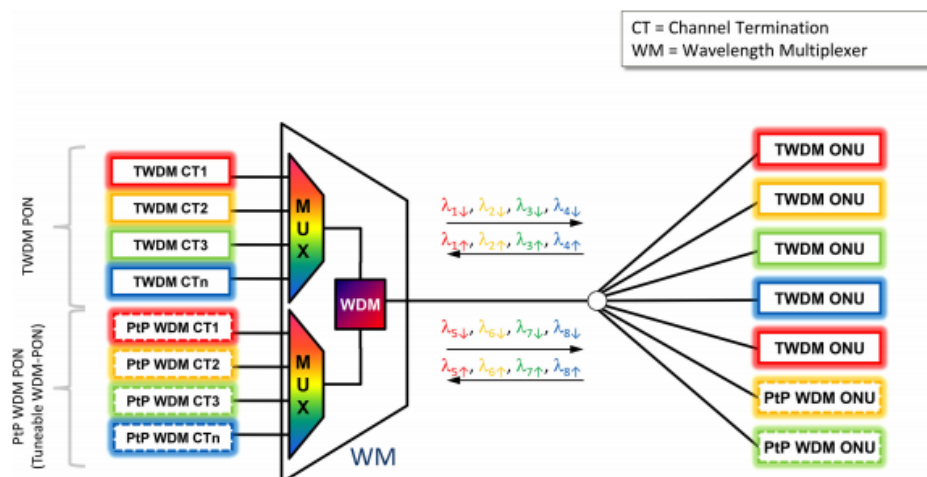
Figure 2.1: NG-PON2 system architecture [2]

Observing the figure, we see the implementation of the TWDM but also for the Point-

to-Point Wavelength Division Multiplexing, PtP WDM, which its importance consists on allowing the NG-PON2 to meet the required demands of the operators for business and backhaul services.

Table 2.1: TWDM-PON data rate options

	TWDM PON	
	Downstream line rate (Gbit/s)	Upstream line rate (Gbit/s)
Basic Rate	9.95328	2.48832
Rate Option 1	9.95328	9.95328
Rate Option 2	2.48832	2.48832

Table 2.2: PtP WDM PON data rate options

	PtP WDM PON
	Downstream/Upstream line rate (Gbit/s)
Class 1	1.2288-1.2500
Class 2	2.4576-2.6660
Class 3	9.8304-11.09
Class 4	6.144

The wavelength plan for both TWDM-PON and PtP WDM PON are specified on the following table, which was projected to enable coexistence through wavelength overlay with legacy PON systems.

Table 2.3: NG-PON2 wavelength bands

Wavelength Compatible Systems	TWDM PON		PtP WDM PON
	Downstream	Upstream	Upstream/Downstream
GPON, RF video, XG-PON1	1596-1603 nm	Wideband option 1524-1544 nm Reduced band option 1528-1540 nm Narrow band option 1532-1540 nm	Expanded Spectrum 1524- 1625 nm Shared Spectrum 1603-1625 nm

Returning back to TWDM-PON, one of it's key challenges consists to underlying tunable components at low cost and to precisely manage and control the λ-domain.

The component that is going to be discussed next, denominated of BOSA, is of great importance for this individual matter, just as it will be seen next.

2.2 BOSA Transceivers

In order to reduce the costs associated to the maintenance of high bandwidth services for Fiber-to-the-Home networks as the already mentioned, NG-PON2, bidirectional communication system has started to be introduced for the PON systems. BOSA stands for bidirectional optical sub-assembly and it consists on the junction of a transmitter optical subassembly TOSA and a receiver optical subassembly ROSA, plus an WDM filter to separate the upstream and downstream wavelengths. The TOSA generally consists of a semiconductor laser (Fabry-Perot or DFB laser) and a laser drive, while the ROSA is composed of a photodiode, either a PIN or an APD, a transimpedance amplifier, a limiting amplifier and finally a clock and data recovery circuit. [3]
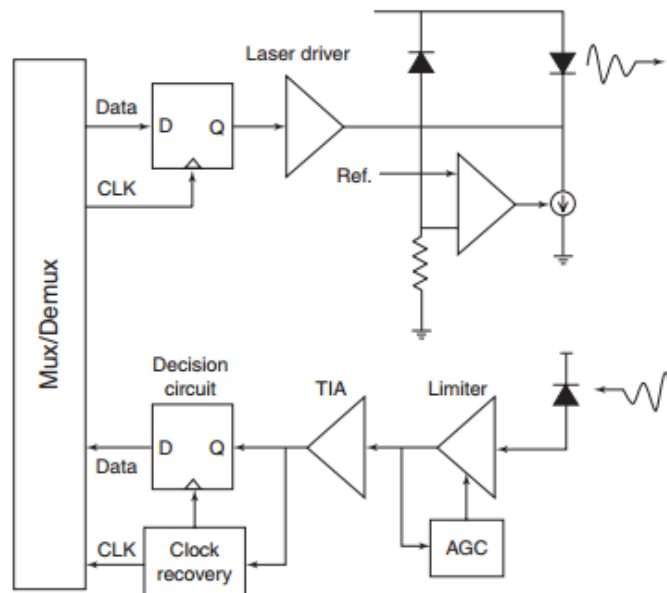
Figure 2.2: Optical transceiver optical diagram [3]

In figure 2.2, it is illustrated the block diagram that constitutes a BOSA transceiver and in 2.3, the physical appearance of one.

Figure 2.3: BOSA transceiver [4]

2.3 Radio Over Fiber

Radio over Fiber consists on modulating the optical signal with an RF signal and then transport that signal through the fiber. This architecture was developed along the concept mentioned above, MIMO. The key resides on the use of optical fiber as a medium for transporting RF signals to and from the RAUs, due to its inherent low-loss characteristics and enormous bandwidth.

As it has been mentioned above, this type of architecture allows several alterations on the communication without having to modify any radio port equipment, such as change the system frequency, modulation format and all this done at a central location. [5].

On the following figure, it is represented, simplistically, the down-link process on a RoF system.
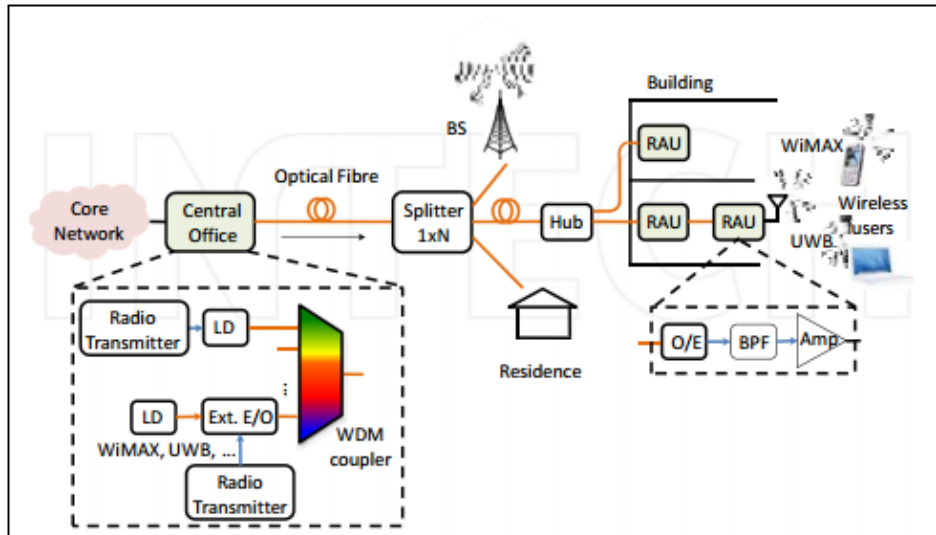
Figure 2.4: Schematic RoF System [6]

The RF signal is transmitted through the optical fiber from the CO and received on the specified RAU, which will then amplify the signal and radiate it through the antenna.

2.4 Advantages

Radio over Fiber can be concluded to offer a vast range of advantages[7], such as:

- **Low Attenuation**: Optical fiber offers low attenuation allowing the transmission of radio signals to a long range, without being required to use regenerators. Comparing with the copper means of transmission, which exhibit much higher losses, fiber really stands out as the obvious better option. The optical fiber used by the different operators, manly multi-mode, introduce approximately loss of 0.2 dB/km and 0.5 dB/km, respectively for the windows of 1550 nm and 1300 nm [8].

- **Large Bandwidth**: High data rate transmission is achieved by the use of optical fiber, which allows for the development of systems which offer large bandwidth, around the two second digits of gigabits.

8

- **Immunity to electromagnetic interference**: The fiber are composed of dielectric materials and therefore doesn't conduct electricity. This characteristic is interesting since it makes the radio signal immune to electromagnetic interferences (**EMI!**) [8]

- **Low costs**: As it has been mentioned already, since the most complex functionalities are performed on the CO, the RAUs become more simple and therefore the implementation costs (**CAPEX!**) decrease significantly. The fact that the RAUs are not as complexed also has influence on the operation costs (**OPEX!**), since the energetic consume decreases. This is obviously an advantages, not only for the costs, but also for the antennas that might be allocated on remote locals, without the energy from the electrical network, and therefore the energetic efficiency becomes even more mandatory.

- **Offer of multiple services**: Radio over Fiber is independent of the technology and therefore allows the transmission of both legacy and new systems. As an example, it allows the coexistence of 2G,3G,4G or even the upcoming 5G.

- **Dynamic Resource Allocation**: Its possible for a dynamic capacity allocation through the use of a Wavelength Division Multiplexing (WDM), since thanks to that equipment it will be possible to redistribute the wavelengths between areas during peak and off-peak times.

2.5   RoF Architectures

Until now, the RoF architecture that as been analysed is the most standard one, but there are several other possible implementations. Next we are going to briefly discuss the architectures IF-over-Fiber and BaseBand-over-fiber.

2.5.1   If-over-Fiber

Intermediate-frequency (IF)-over-fiber corresponds to a different architecture from the simple analogue version. Basically, on this implementation the RF signal is downconverted to a lower intermediate frequency, that is posteriorly used to modulate the laser transmitter. When the signal is detected by the photodiode receiver, it is then upconverted to the required RF frequency before being wirelessly transmitted [9].

The advantages of this implementation is that it lowers the frequency of operation of both the laser transmitter and photodiode receiver but also minimizes the effects of fiber chromatic dispersion [1]. As a drawback, it requires the use of additional RF components on the antennas, such as local oscillators (LO) and filters, which increase its complexity. Overall this implementation presents advantages and is specially of use for milimeter-wave-over-fiber system, whose are going to be discussed later on.

2.5.2   BB-over-Fiber

Another technique that can be used to transport the data carrying of the radio signals is denominated of baseband (BB) over fiber. Basically the radio information is transported to the BS as a time division multiplexed (TDM) digital data stream and is later demultiplexed into individual channels and up converted to IFs, and posteriorly up converted to the required radio frequency, with an LO at the antenna. In the case of the upstream direction, it can be

achieved by down conversion at the BS the wireless carriers, to the baseband before being transmitted to the CO [10].

On the following figure, there is a representation of the different architectures that have been discussed.
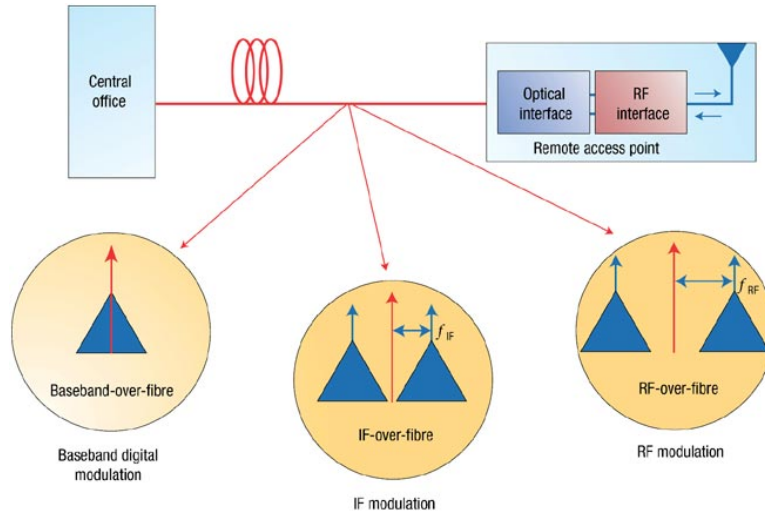
Figure 2.5: RoF Architectures [11]

2.6   Digital RoF

The processing of digital signals has revolutionized the modern communications systems, bringing a lot of advantages, such as immunity to noise, flexibility enabling the implementation of more robust architectures of radio-over-fiber and therefore presenting themselves has a viable alternative to the analogue systems. DRoF stands therefore for digitized radio-over-fiber, and in comparison to the analogue version, it transmits digital input through the fiber instead of an analogue signal, as it has been mentioned.

On the digital transmission, the degradations on the optical field that affect the RoF system are minimized and consequently the signal performance is a lot better and the range onto which it can be transmitted increases [12]. Adding to all of this, the fact that the costs associated to the Digital-to-Analogue Converters (DACs and ADCs) have dropped has made possible the installation of such components, not only on the CO but also on the several BSs, and therefore allowing for the transmission between the transmitter and the receiver to be all done on the digital domain.

The process for the downstream consists on the digitalization of the electrical signal by an ADC with a sampling frequency defined by the Nyquist theorem [13]. The sequence of serial bits is then modulated by an optical carrier, transmitted through the fiber and then detected by the receiver, on which the signal is converted again to the electrical domain, followed by the conversion to analogue by a DAC. On the final stage the signal is propagated by the antenna. The upstream process, from the antenna to the CO follows the same process. On the following figure is represented the basic architecture of an DRoF system:
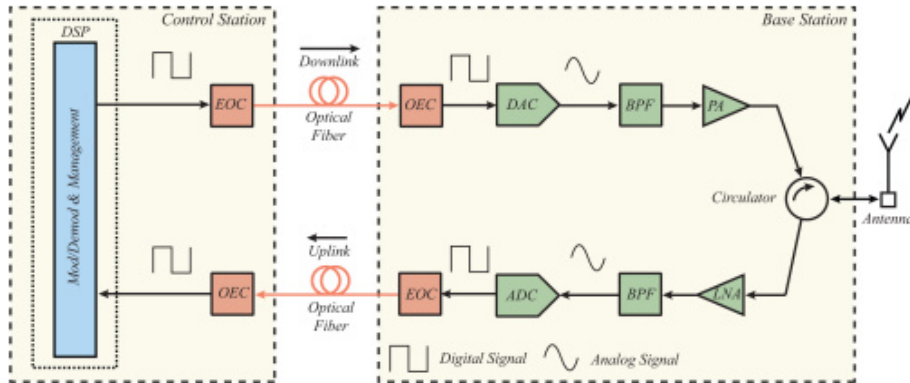
Figure 2.6: Digital Radio-over-Fiber Architecture [14]

The limitation of this technique is related to the ADC/DAC sampling frequency. This problem is not easy to solve because equipment with such high sampling frequencies have high power consumption and are relatively expensive. Down-conversion techniques of the RF signal can be used to lower the ADC/DAC sampling frequency requirements [14].

Standardizations between the interface central baseband module and remote RF of digital RoF architecture has been made, with the most important being the Open Base Station Architecture (OBSAI), but specially the Common Public Radio Interface (CPRI). Due to the importance of the last protocol, it will be explained on a later section.

2.7 Types of Modulation

Directly modulating the intensity of the light source with the RF signal itself at the transmitter and then use direct detection at the photodetector to cover the RF signal is the simplest method for optical distribution of RF signals which falls under the IM-DD category. Three ways will be studied that are able of achieving this. The first consists on letting the RF signal directly modulate the lasers diodes current, while the second option requires the operation of the laser on continuous wave (CW) mode and then the use of an external modulator such as the Mach-Zehnder modulator (MZM) to modulate the intensity of the light. The third consists as well on external modulation but with a reflective semiconductor optical amplifier.

In the first two cases the modulating signal is actually the RF signal to be distributed, which requires some pre-modulation with data prior to its transmission. For that reason the RFoF requires high-frequency electro-optic equipment at the headend. After the signal gets propagated through the fiber and direct detected on the photodiode, the photocurrent is a replica of the modulating RF signal applied to the laser or to the external modulator at the headend. In case of the RF signal being used to modulate the transmitter, itself is modulated with data and then the detected RF signal at the receiver will be carrying the same data, and therefore the modulation format of the data preserved.

Comparing the direct with the external modulation, we conclude that the direct is rather simple and cost effective, but on the other hand since the lightwave modulation is performed

11

by an additional component on the external modulation, it offers certain advantages, such as reducing the effect of frequency chirp (the spreading of the lightwave frequency content due to the direct modulation), which is greatly responsible for increasing the fiber dispersion, enabling higher frequency modulation, beyond the limitation for the modulation bandwidth of semiconductor lasers and also allowing for a lower noise and an higher link gain. The option we shown for the externally modulated link, was done using MZM which is based on electro-optic effect, but electro-absorption modulators (EAMs) are also of interest as they can be integrated with semiconductor lasers. There has been done some studying regarding a different a new type denominated of Reflective Modulators, which can be combined with semiconductor amplifiers in order to boost the modulated lightwave which was reflected. This implementation can be really interesting for remote modulation, where the signal picked up by a remote antenna can be applied to such a modulator in order to modulate a CW light-wave generated centrally, and the reflected lightwave comes back to the central location is impressed with the received wireless signal.

Another option for the links consists also on external modulation, but instead of using a MZM to use reflective semiconductor optical amplifier (RSOA). But for this specific case this is only a possibility for the uplink direction, since it uses optical light from the CU and therefore does not require an optical source at the RAUs [15]. The downside though consists on the fact that it will require the use of an optical circulator, just so it's possible to separate the incident light from the reflected, which therefore will increase the complexity and consequently the cost of the optical links. In order to minimize the noise that arises from amplified spontaneous emission (ASE), some form of optical filtering is required in the optical fiber network [16]. But the fact that the optical networks are already using optical filtering, with the WDM multiplexers/demultiplexers in order for a single CU to be able to support several RAUs. The fact that RSOA link has no pre-assigned wavelength, in contrast to the other links type, is a major advantage, provides a greater flexibility and leads to cost-effective production, especially for large networks. The flexibility component makes it so that it is feasible to control and allocate the wavelengths to each RAU, leading therefore to the possibility of a flexible and dynamically reconfigurable network.

2.8   Impairments

Above has been explained most of the advantages that arose from the use of radio over fiber, but this architecture also presents some inherent limitations. Because of the fact that RoF involves analogue modulation, and also detection of light, it is manly an analogue system. Consequently, like any other analogue system, it is affected by impairments such as the noise and distortion, which will deteriorate its performance, limiting the Noise Figure (*NF*) and Dynamic Range (DR) [17].

The components on the RoF's system that add noise to the system are the laser, photodiode, amplifier and fiber and therefore a characterization will be made regarding these elements. But the DRoF systems cannot be forgotten, and therefore the presence of Digital-to-Analogue and Analogue-to-Digital Converters,respectively (DAC and ADC), is also necessary to take into the account, because of the noise associated to them.

The DR is a very important parameter for cellular communications system, since the power on BS from the several Mobile Units (MU) varies widely, because depending on the distance between the MU and BS, the power of the radio signal received will greatly differ and if the DR is lower, that will severely limit the kilometres that each antenna can actually cover. Relatively to the noise, on the following section, more interest is going to be given in analysing such phenomenons.

2.8.1 Transmitter Noise Source

On this subsection, some study regarding the impairments added by the light source on the performance of the system are going to be discussed. Depending on the type of the laser, its parameters and the type of modulation selected ,certain impairments will affect the performance of the system.

☐ **Laser RIN**

The relative intensity noise measures the strength of an output intensity fluctuation of a laser relative to the square of the average optical output power [18]. RIN is highly dependent on the laser design and is therefore a function of several physical operation parameters in the device, just like the temperature, modulation frequency, cavity path length or even the active medium and injection current [19].

☐ **Chirp**

The chirp frequency of directly modulated semiconductor laser in interaction with chromatic dispersion causes distortions of the signal travelling along the optical fiber. The chirp occurs because the direct intensity modulation leads to some variation of carrier concentration in the laser active regions, which therefore affects the refractive index and consequently the frequency of the optical signal generated. The chirp of single frequency laser can be described with the following equation:

$$\Delta v(t) = \frac{\alpha}{4\pi}\left(\frac{d}{dt}[ln(P_L(t)) + kP_L(t)]\right) \tag{2.1}$$

Where $\Delta v(t)$ is the instantaneous frequency deviation, is the line enhancement factor, k is the adiabatic chirp coefficient, and P_L(t) is the laser output power. The first term on the above expression, which is proportional to the derivative of the logarithmic output power is called transient chirp, while the second, directly proportional to the power, is denominated of adiabatic chirp. The equation mentioned above was derived for the Fabry-Perot (FP) lasers, but it is also widely used as an approximation for DFB lasers. For very low modulation frequency, the chirp induced by temperature variations of the laser chip, can also be observed but this effect is not essential for high-speed laser transmitters. The laser chirp may be eliminated by applying the external modulator, by reducing the dispersion (compensated), or simply by dividing the span by regenerators into shorter ones.

☐ **Clipping**

In order for the laser to operate, a minimum current has to be applied on it, and that level is defined as the threshold bias current. Above this level, starts the linear operation of the laser, but the problems start to arise for high levels of power input signal that cause

power peaks and therefore extend to the nonlinear area of the laser-biasing curve, which is responsible for the high level distortion on the output signal.

☐ **Intermodulation Distortion**

The nonlinear effects induced by the optical modulators cause intermodulation distortion (IMD) and therefore result in signal degradation [20]. These affects are more noticeable on the presence of external modulation, but the direct modulation has the limitation of permitting a low modulation band and an high relative intensity noise (RIN).

The most common intermodulation distortions correspond to the second and third order, and their location on the spectrum are obtained by injecting a two-tone signal into a device under test (DUT). In case the of a perfectly linear amplifier the output signal would include two tones at the exact same frequency of the input signal, but at the amplified output power. But a more realistic amplifier, which will always have some level of nonlinearity, will produce additional content at other frequencies other than the two mentioned previously, as it can be seen on figure 2.3.
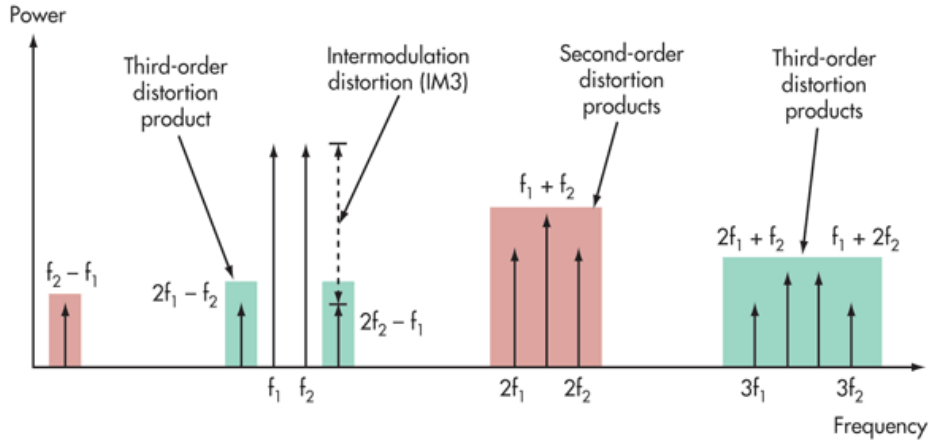
Figure 2.7: Two-tone harmonic distortions [21]

Second harmonics occur at multiples of the fundamental tones, such as $2f_1$ and $2f_2$, and for third harmonics it will be $3f_1$ and $3f_2$. Additionally, the system will produce second and third order distortions products at each combination of first and second-order products. While the distortions of second order can be easily removed by a filter, the same can't be mentioned about the third-order intermodulation distortion, as it lies very close to the fundamental carriers and therefore impossible to eliminate them simply by the use of RF filters [22].

In order to characterize the performance of the radio over fiber depending on the third order distortion there is a measurement denominated of third-order intercept (TOI).The product of the intermodulation of the third order is given by,

$$IM(dBm) = 3P_{in} - 2PI \tag{2.2}$$

Where, IM corresponds to the power of the intermodulation product, P_in is the power of the input signals and IP the interception point.

Lastly the SNR generated by the intermodulation can be obtained by the following equation 2.3:

$$SNR_{IM} = 2IP - 2P_{in} \qquad (2.3)$$

2.8.2 Degradation due to optical fiber

On the optical domain the degradations suffered by the signal are manly due to the effects of both attenuation and dispersion, which impacts the transmission of high work frequency systems with elevated bit rates, since the system will require high transmitted power and therefore increase the probabilities of the system suffering from nonlinearities.

On monomode fibers, the chromatic dispersion impacts a lot the performance of the system, since it does flat the pulses of information (0s and 1s), making them harder to distinguish at the far end of the fiber. On multimode fibers, the dispersion observed is the modal, which consists on the spreading of the signal in time because the propagation velocity of the optical signal is not the same for different modes.

□ **Chromatic Dispersion**

Single-mode fibers only carry the lowest-order mode, since the cuttoff condition for the next modes, V ¡ 2.405 is guaranteed, and therefore only HE_{11} is propagated and TE_{01} and TM_{01} are not. Intramodal dispersion is also denominated of group velocity dispersion, since the fact that different frequency components of an optical signal have a different group velocity and therefore result on the intramodal dispersion. There are two main components that are responsible for this type of dispersion and those are, material dispersion and waveguide dispersion. Material dispersion occurs when the dieletric constant and the refractive index vary with the wavelength, while material dispersion is related to the structure of the waveguide, since the propagation parameters are dependent on the structure of the waveguide.
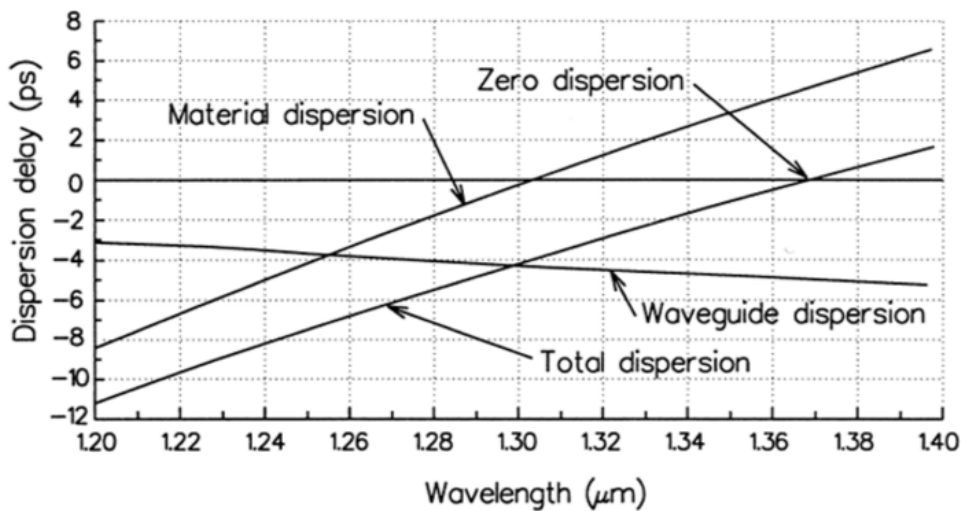

Figure 2.8: Dispersion Coefficient on Single-Mode fibers [23]

☐ RF Power Fading

RF Power Fading consists on the effect of the chromatic dispersion in analog optical links and it has been a subject of greater interest in the past few years. Each spectral component experiences different phase shift because of chromatic dispersion resulting in relative phase differences between each sideband and the carrier.

The most commonly optical links used in order to impose the RF signal onto the optical carrier, incorporate a MZM. Performing this operation with MZM has the advantage that it doesn't add even-order distortion to the signal upon detection on the photodiode, but it has the disadvantage of its output result in a dual sideband (DSB) signal [24], which is negatively affected by chromatic dispersion.

The behaviour of the power of a RF signal, for a fixed radio frequency, can be approximated by 2.4 [25],

$$P_{rf} \propto cos[\frac{\pi LD}{c}\lambda_c^2 f_r f^2]$$
(2.4)

The fact that the signal power varies as a cosine function, as it is shown on equation 2.4, indicates that at certain fiber lengths power cancellation will happen,

$$L = \frac{Nc}{2D\lambda_c^2 f_{rf}^2}, \quad N = 1, 3, 5, 7, ...$$
(2.5)

☐ Modal Dispersion

The group velocity and the propagation of the different modes defines the modal dispersion, which basically is a multipath phenomenon, independent of the characteristics of the optical signal being transmitted. The following equation represents the difference in propagation delays between the fastest and slowest modes,

$$\delta_{tw} = \frac{n_1 - n_2}{c}\left(1 - \frac{2}{v_{max}}\right)$$
(2.6)

☐ Attenuation

There exist several losses mechanisms that are responsible for the attenuation of the optical signal while it is being propagated along the fiber. The fact that optical receivers require a minimum amount of optical power to recover the information that is transmitted, limits the maximum distance that an optical signal can be transmitted through the fiber and therefore for long-haul optical communications systems, fiber loss becomes a intrinsically limiting factor. If at the transmitter side an optical power signal with power P_{in} is launched into an optical fiber of length L, after propagating through an optical fiber, the optical power received at the end of the fiber is,

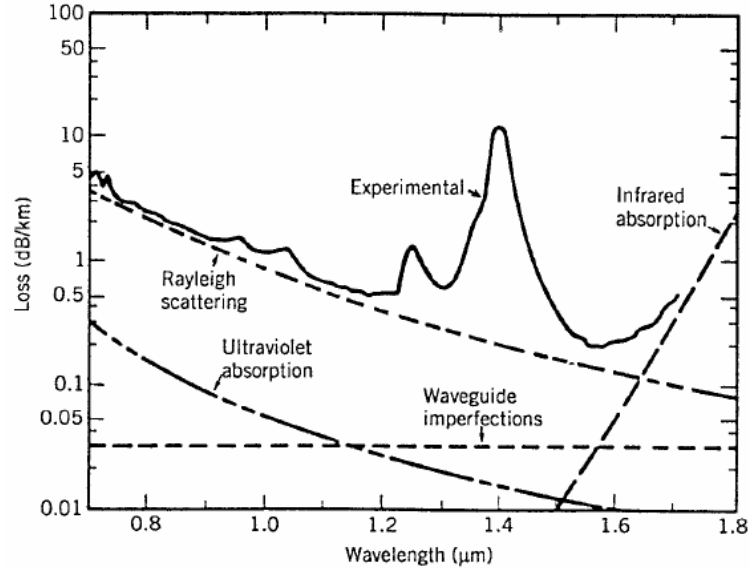$$P_{out} = P_{in}exp(-\alpha_f z)$$
(2.7)

Figure 2.9: Optical fiber loss spectrum [26]

There are three major factors that contribute to the fiber loss spectrum, and those are: material absorption, waveguide imperfections and Rayleigh scattering, though in practice, fiber connectors and nonlinear effects also contribute for power losses. The material from which the fiber is composed is silica, which when fused with impurities such as water and certain metals, is responsible for the material absorption. On the ultraviolet region, strong absorption peaks are created due to the fused silica electronic resonance, while molecular vibration is responsible for the absorption of infrared wavelengths. In the early years much of the improvement in reducing fiber loss were obtained by the material purification. Rayleigh scattering happens due to the fluctuation in fiber materials. Even though the fluctuations are on a scale smaller than the wavelength of the optical signal, the random changes still lead to light scattering, and by the following formula it's possible to calculate its value,

$$\alpha_R = \frac{C_R}{\lambda^4} \tag{2.8}$$

On an ideally concept, optical fiber would be a perfect cylinder with constant core diameter and a smooth core-cladding interface [3]. However, certain imperfections such as the variation of the core radius or bending will be responsible for optical power loss. Small bends on the optical fiber can lead to the scattering of a part of the optical power into the cladding layer. The presence of refractive index inhomogeneities will be responsible for the coupling between guiding modes and cladding mode. In order to reduce the losses originated by these factors, the process of fiber drawing is closely monitored to ensure that the variations on the fiber diameter are really low, and during the installation minimizing the random axial distortions is a priority. Modern optical networks use multiple stages of optical amplifiers to compensate for the fiber loss, though they are responsible for amplification of spontaneous noise, but there is a limit on the maximum reach that an optical communication system can support independently of how many optical amplifiers are used.

17

2.8.3 Receiver Noise Sources

The degradations that happen on the receiver are originated by the fotodetector as a function of the thermal noise of the electrical circuit but also from the shot noise existent due to the aleatory reception of photons. The two main types of photodetector correspond to the PIN and APD,

The thermal noise happens due to the random collisions of carriers with crystal atoms which permanently vibrate, that create thermal agitation [27].The following equation is used to obtain it's value,

$$N_{th}^2 = \frac{4k_BT}{R_L}F_n\Delta f \tag{2.9}$$

Where, I_d corresponds to the dark current, q is the electron charge, Δf bandwidth, R_L is the charge resistance to convert the output current to the signal voltage, R the responsivity of the photodetector and B_DR the total transmitted rate.

The shot noise can be calculated by the following expression, where F_n corresponds to the noise figure, T the temperature of the photodetector and K_B the Boltzmann constant.

$$N_s^2 = 2q(I_d + I_p)\Delta f . I_p = RP_{in} \tag{2.10}$$

2.8.4 Digital RoF systems noise

When comparing the SNR between analogue and digital architecture of the RoF system, the impact of the ADC/DAC have to be taken into account on the former, so therefore the SNR on the Digital RoF systems cannot be obtained by the equation (2.5).

☐ **ADC jitter noise**

The jitter noise is defined by the temporal delay between the ideal instant for sampling, and its SNR can be given by the following equation,

$$SNR_j = \frac{P_S}{N_j} \tag{2.11}$$

Where P_S corresponds to the power of the signal and N_J the power of noise during one period of sampling. This last variable can be obtained by equation (2.7)

$$N_j(n) = E[E_t(n)]^2, E_t(n) = y(t_n - \tau_n) - y(\tau_n) \tag{2.12}$$

On the case that the signal we are dealing with is sinusoidal, the mean of the noise power can be approximated by the following equation,

$$\overline{N}_j = 2\pi^2 f^2\sigma_t^2 A^2 \tag{2.13}$$

Where, σ_t is the medium square error of the sampling instant.

☐ **Quantization noise**

The difference in voltage between the input signal (y_n) and the output signal (y_q) corresponds to the quantization noise. For an ideal ADC, this noise would be uniformly distributed between $-\frac{1}{2}$ and $+\frac{1}{2}$ of the Least Significant Bit. With equation 2.9, it's possible to obtain the quadratic mean error [28],

$$RSM_{eq(n)} = \sqrt{2^{Q-1} \int_{-\frac{1}{2Q}}^{\frac{1}{2Q}} e_q^2(n) = \frac{1}{\sqrt{32^q}}} \tag{2.14}$$

The relation of the signal quantization noise is given by the fraction between the quadratic mean error of the input signal and the quantization,

$$SRN_q = 20log_10(3^{1\frac{1}{2}\sqrt{32^Q}}) = 6.0206Q(dB) \tag{2.15}$$

But for an M-QAM, the quadratic mean error, is not evenly distributed and it's value corresponds instead to,

$$RMS_{x(n)} = \left(\frac{\sqrt{M+1}}{3\sqrt{M}-3} \right)^{\frac{1}{2}} \tag{2.16}$$

which gives the following equation for the SNR,

$$SNR_Q = 20log_{10} \left(\left(\frac{\sqrt{M}+1}{3\sqrt{M}-3} \right)^{\frac{1}{2}} \sqrt{32^Q} \right) = 6.02Q + 10log \left(\frac{\sqrt{M}+1}{\sqrt{M}-1} \right)(dB) \tag{2.17}$$

From this equation it can be concluded that the resolution of the ADC affects greatly the quantization noise generated, since with the increase of one bit, it means a raise of 6 dB on the SNR [29].

2.9 CPRI

CPRI was established in 2003 by base station vendors, such as Ericsson, Nokia Siemens Networks, Alcatel Lucent, NEC, and Huawei Technologies. The CPRI protocol consists of three planes, the User Plane that carries the IQ data, a Control Plane that provides control signalling to and from the remote radio and a Sync Plane that is responsible to keep the baseband and remote radio in sync. This standardization was done in order that it would be done for chipset vendors to create components that could be used by any radio equipment vendor. However, the standard is not completely open, which means certain aspects of the signalling are vendor specific, so mixing radios and baseband units from different vendors is not guaranteed to function [30]. Regarding the CPRI protocol, it is a full duplex serial data stream, which means there is a transmission and receiver fiber. Since CPRI is a synchronous protocol, the baseband must establish synchronization with the remote radio before communications can be established. One CPRI stream is able of supporting several IQ data flows

to several different radios and since operators generally use multiple radios at each cell site (different carrier frequencies) it means that the CPRI can have a separated IQ data flow for each one of those radios. The following figure illustrates how the CPRI protocol works from getting the RF signal transmitted towards the IP backhaul, trough fiber, and the vice versa.
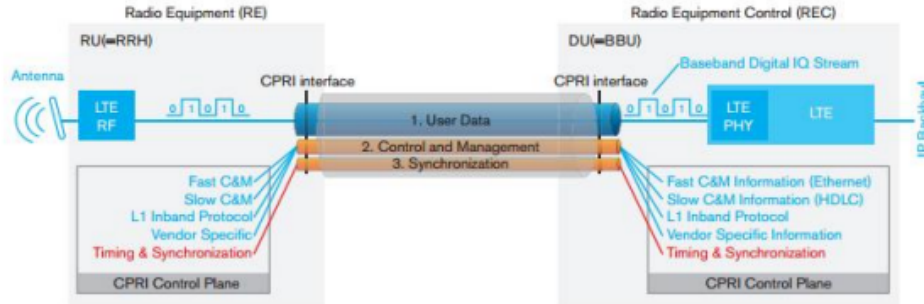

Figure 2.10: CPRI transport concept [31]

The RF signal is digitized via the RRH and is commonly referred as Digital Radio over Fiber (DRoF). The following step consists on wrapping the signal into the CPRIs protocols User Data signal flow, known as IQ Data. The I refers to phase and the Q to quadrature. The same process takes place as traffic enters via the IP backhaul. The signal is wrapped again within the user data signal flow of the CPRI protocol on the Digital Unit and when this data is received by the RRH it is then converted back to analogue so it can be amplified and then transmitted over the air, so it can eventually reach the User Equipment (UE).

2.10 Milimeter-Wave-over-Fiber Systems

One of the applications of the RoF system consists on the generation of mm-wave signals. Due to the scarcity of spectrum in the microwave frequency band, especially in the lower region up to 6 GHz, which is the frequency of operation of several mobile and wireless communications services, has led to the interest in milimeter-wave communication system. On this region (30GHz to 300GHz) [32] there are large bands of frequency available, which offers the possibility of wide-bandwidth and high-data-rate communications, which have been proposed to be a decisive part of the 5G mobile network in order to provide multi-gigabit communication services such as high definition television (HDTV) and ultra-high definition video (UHDV) [33].

The main characteristics of the mmWave are the following:

- **Path Losses**: Compared to other communications system, the milimeter wave communications suffer from huge propagation loss in using lower carrier frequencies, due to the rain attenuation and atmospheric/molecular absorption. However these affects are not as significant for cell sizes on the order of 200m, with the application of smaller cells in order to increase the spectrum efficiency since the path loss then added by the rain and atmospheric is no longer significant. Therefore mmWave communications are manly used for indoor environments, and small cells access and backhaul with cells sizes on the order of 200m [34].

- **Directivity**: The mmWave links are inherently directional, which means that an high gain is obtained at a certain direction and that for all other directions there exists a very low gain. This is achieved with electronically steerable antenna arrays can be realized as patterns of metal on circuit board [35], whose transmitted signal is controlled by the phase. In order for the transmitter and receiver to project the beam towards each other, procedure of beam training is required.

- **Sensivity to Blockage**: Electromagnetic waves have weak ability to diffract around obstacles with a size significantly larger than the wavelength. With a small wavelength, links in the 60 GHz band are sensitive to blockage by obstacles , such as humans and furniture.

2.11 Application of mmWave Communications for 5G

The large band in the mmWave bands promotes the usage of mmWave communications in the 5G cellular access , since it has been concluded that, as long as the infrastructure is densely employed, mmWave cellular networks have the potential for high coverage and capacity. Certain experiences have been made, and it has been demonstrated the efficiency of the system at frequencies of 28GHz and 38GHz, with cell sizes at the order of 200m. It has also been shown that the capacity gains obtained with the directional antennas pointing on arbitrary angles is greatly superior to the gain obtained for the 4G LTE networks, around the 20 times greater actually. This value can be further improved if the directional antennas are pointed in the strongest transmit and receive directions. On the following figure is represented the network architecture of the mmWave 5G,
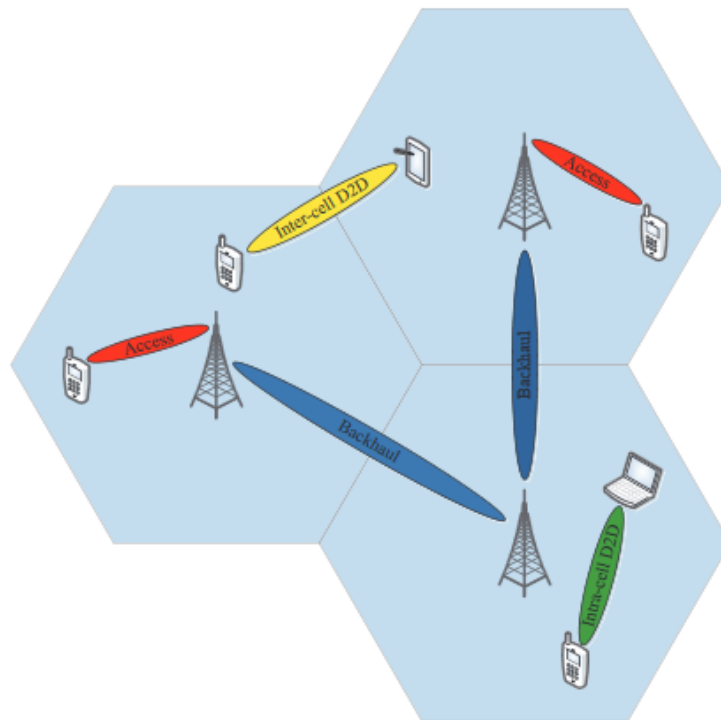

Figure 2.11: MmWave 5G cellular network architecture with D2D communication [34]

On the figure it is shown device-to-device (D2D) communications , which in close proximity have the feature of not only saving power, but also improve spectral efficiency,and therefore will be a feature of the mmWave 5G cellular network architecture, allowing the support of applications that involve communication between nearby devices. In D2D communication underlaying cellular networks, there are 4 resource allocation methods: cellular mode, dedicated resource mode, reusing the resource of only one cellular user and lastly reusing the resources of more than one cellular user [36]. The last two modes bring interference to the system because they don't use orthogonal resource, and D2D users share the same resource with cellular users. The interference can be divided in two categories, intra-cell and inter-cell. As the name suggests the first consist on interference between cellular users and D2D users, but

the inter-cell is not as easily explained. It can consist on the interference between neighbours D2D users and attached cellular users,or the interference between neighbour D2D users and attached D2D user, or the interference between neighbour cellular users and attached D2D users and lastly the interference between neighbour cellular users and attached cellular users. Considering the case presented on the figure, with the inter-cell, intra-cell D2D, backhaul and access link enabled in the mmWave band, in order to unleash the potential of this architecture its required to have an efficient and flexible radio resource management schemes, such as power control, user access and transmission scheduling.

The fact that it will be required to deploy densely the next generation of cellular systems (5G) with small cells, it would be costly if the connection between 5G and to the network by using fiber based backhaul [37], so high speed wireless backhaul is not only more cost-effective, but also more flexible and easier to deploy and therefore seems to be the better solution.
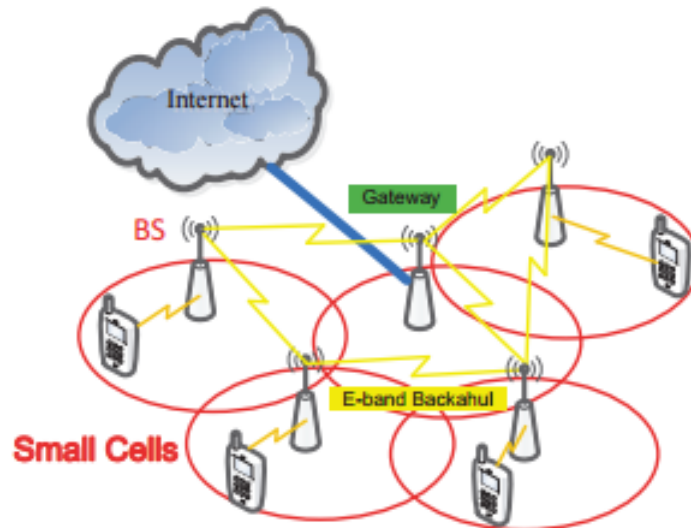

Figure 2.12: E-Band Wireless Backhaul for small cells densely employed [34]

As shown in figure 2.8, using the E-band (71-76 GHz and 81-86 GHz) can be a promising solution for small cells, providing several G-bps data rates.

Chapter 3

Simulation

Simulating a Radio Over Fiber Analogue System was one of the objectives presented for the development of this dissertation. We had the option on performing the simulation on an established platform (**VPI!**) or to implement a simulation environment with the help of Matlab and the latter option ended being the one selected.

Briefly explained, in order to simulate the RoF System, several steps had to be followed, which can be observed on 3.1. The first consisted on generating the RF signal, with the desired frequency and characteristics (format modulation and pulse shaping). The second phase corresponded on modelling the propagation of the RF signal on the optical system, while the last phase consisted on receiving it and analysing the reception conditions.

The process followed for the implementation on Matlab is represented on the following block diagram:
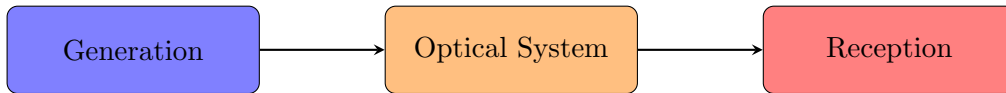

Figure 3.1: Simulation main 3 steps

The following sections are going to be about describing the process followed in detail and the choices made on implementing for each relevant block of the diagram.

3.1 Creating the signal

In order to generate a RF signal on Matlab several steps had to be followed. The first consisted on generating randomly and with the same probability, '0' and '1' bits. The bits vector generated then goes through an I/Q Mapper, where the I stands for In-Phase and Q for Quadrature. What this means is that the signal is now separated into two channels and depending on the selected modulation format and the defined amplitudes for the symbols's constellation, the I/Q signals varies. With the I/Q signals generated the next phase consisted on applying pulse shaping. Pulse shaping is applied in order to change the waveform of the transmitted pulses, in order to make it better suited to the desired communication channel.

Generating the RF signal is not only of importance for the simulations purpose, but also for the experimental work, since the RF signal will have to be loaded into an Arbitrary Waveform Generator AWG, which will be responsible for the transmission of the RF signal to the optical system. The characteristics of the pulse shaping and the respective up-sampling were defined based on the predefined sample rate range of the AWG instrument.

The final step consisted on mixing both IQ signals, using the following formula, in order to obtain the desired RF signal:

$$Modulation\ Carrier\ RF = I \times cos(2\pi t) + Q \times cos\left(2\pi t + \frac{\pi}{2}\right) \tag{3.1}$$
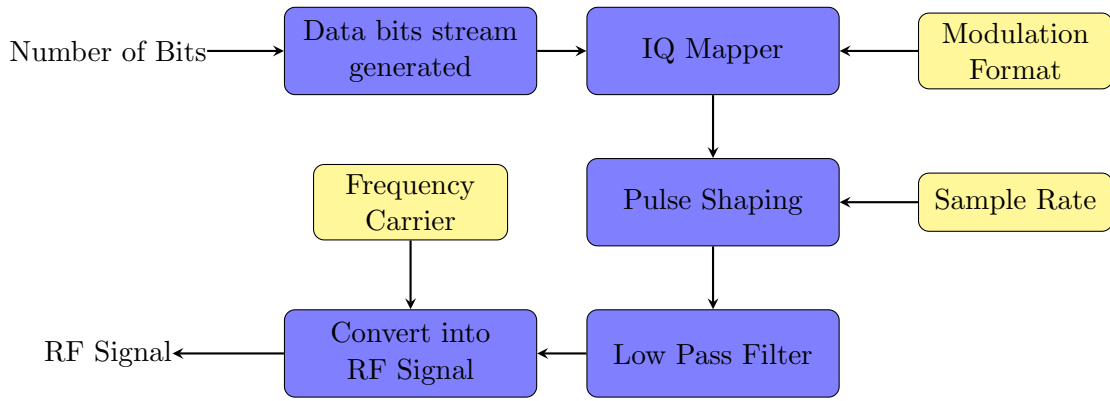

Figure 3.2: Generated RF Signal Block Diagram

3.1.1 Modulation Format

In order for information to be carried in single-mode optical fibers, the optical field, has three physical attributes that can be used only intensity, since coherent reception was not used.

But the attributes selected for the simulation were both intensity and phase for the generation of the electrical signal, since the most important modulation formats implemented were the 8-PSK (phase) and M-QAM(intensity and phase), but since the system doesn't detect phase, the electrical signal transmitted could not be a complex signal.

The objective of having several modulation formats implemented was basically to observe the performance obtained for each one and therefore be able to draw a comparison between them.

3.1.2 Multilevel Signals

□ QPSK

Phase Shift Keying as the name indicates is a phase modulation algorithm. The carrier wave's phase is modulated to encode bits of digital information in each phase change. QPSK, stands for Quadrature Phase Shift Keying and uses 4 states.

Table 3.1: QPSK symbols amplitudes

	00	01	10	11
Ix	$\frac{\sqrt{2}}{2}$	$-\frac{\sqrt{2}}{2}$	$\frac{\sqrt{2}}{2}$	$-\frac{\sqrt{2}}{2}$
Qx	$\frac{\sqrt{2}}{2}$	$\frac{\sqrt{2}}{2}$	$-\frac{\sqrt{2}}{2}$	$-\frac{\sqrt{2}}{2}$

☐ **M-QAM**

QAM stands for Quadrature Amplitude Modulation and it is a signal in which two carriers shifted in phase by 90 degrees are modulated and which output consists on variations on both amplitude and phase, which means there exists a mixture of both amplitude and phase modulation.

Generally a M-QAM constellation is arranged in a square grid with the same space vertically and horizontally and the number of points is equal to a power of 2, i.e. 4,16,32,64 and so on.Utilizing the following equation you can relate the number of states with the amount of bits that the symbols will require ,n,

$$Number\ of\ States = 2^n \tag{3.2}$$

With the increase of the number of points, the transmitted bits per symbol also increase, however because of that fact, the points are closer to each other and more susceptible to noise, which can therefore cause data errors. So high order versions of QAM are only used when an high there is a sufficiently high signal to noise ratio.

In table 4.3 and 3.3 it's represented the I/Q Mapper implemented for 16-QAM and 64-QAM, respectively.

Table 3.2: 16-QAM symbols amplitudes

	0000	0001	0010	0011	0100	0101	0110	0111
Ix	1	$\frac{1}{3}$	-1	$-\frac{1}{3}$	1	$\frac{1}{3}$	-1	$-\frac{1}{3}$
Qx	1	1	1	1	$\frac{1}{3}$	$\frac{1}{3}$	$\frac{1}{3}$	$\frac{1}{3}$
	1000	**1001**	**1010**	**1011**	**1100**	**1101**	**1110**	**1111**
Ix	1	$\frac{1}{3}$	-1	$-\frac{1}{3}$	1	$\frac{1}{3}$	-1	$-\frac{1}{3}$
Qx	-1	-1	-1	-1	$-\frac{1}{3}$	$-\frac{1}{3}$	$-\frac{1}{3}$	$-\frac{1}{3}$

☐ **M-PSK**

Phase Shift Keying formats consists on the multiplication of a generally complex symbol waveform by an alphabet of complex numbers, which all lie on the unit circle. The phase in an M-ary PSK is therefore divided into M evenly levels for M different waveforms.

Table 3.4: 8PSK symbols amplitude

	000	001	010	011	100	101	110	111
Ix	$\frac{\sqrt{2}}{2}$	1	-1	$-\frac{\sqrt{2}}{2}$	0	$\frac{\sqrt{2}}{2}$	$-\frac{\sqrt{2}}{2}$	0
Qx	$\frac{\sqrt{2}}{2}$	0	0	$-\frac{\sqrt{2}}{2}$	1	$-\frac{\sqrt{2}}{2}$	$\frac{\sqrt{2}}{2}$	-1

Table 3.3: 64-QAM symbols amplitude

	000000	000001	000010	000011	000100	000101	000110	000111
Ix	1.1501	1.1501	0.8215	0.8215	1.1501	1.1501	0.8215	0.8215
Qx	1.1501	0.8215	1.1501	0.8215	0.1643	0.4929	0.1643	0.4929
	001000	**001001**	**001010**	**001011**	**001100**	**001101**	**001110**	**001111**
Ix	0.1643	0.1643	0.4929	0.4929	0.1643	0.1643	0.4929	0.4929
Qx	1.1501	0.8215	1.1501	0.8215	0.1643	0.4929	0.1643	0.4929
	010000	**010001**	**010010**	**010011**	**010100**	**010101**	**010110**	**010111**
Ix	1.1501	1.1501	0.8215	0.8215	1.1501	1.1501	0.8215	0.8215
Qx	-1.1501	-0.8215	-1.1501	-0.8215	-0.1643	-0.4929	-0.1643	-0.4929
	011000	**011001**	**011010**	**011011**	**011100**	**011101**	**011110**	**011111**
Ix	0.1643	0.1643	0.4929	0.4929	0.1643	0.1643	0.4929	0.4929
Qx	-1.1501	-0.8215	-1.1501	-0.8215	-0.1643	-0.4929	-0.1643	-0.4929
	100000	**100001**	**100010**	**100011**	**100100**	**100101**	**100110**	**100111**
Ix	-1.1501	-1.1501	-0.8215	-0.8215	-1.1501	-1.1501	-0.8215	-0.8215
Qx	1.1501	0.8215	1.1501	0.8215	0.1643	0.4929	0.1643	0.4929
	101000	**101001**	**101010**	**101011**	**101100**	**101101**	**101110**	**101111**
Ix	-0.1643	-0.1643	-0.4929	-0.4929	-0.1643	-0.1643	-0.4929	-0.4929
Qx	1.1501	0.8215	1.1501	0.8215	0.1643	0.4929	0.1643	0.4929
	110000	**110001**	**110010**	**110011**	**110100**	**110101**	**110110**	**110111**
Ix	-1.1501	-1.1501	-0.8215	-0.8215	-1.1501	-1.1501	-0.8215	-0.8215
Qx	-1.1501	-0.8215	-1.1501	-0.8215	-0.1643	-0.4929	-0.1643	-0.4929
	111000	**111001**	**111010**	**111011**	**111100**	**111101**	**111110**	**111111**
Ix	-0.1643	-0.1643	-0.4929	-0.4929	-0.1643	-0.1643	-0.4929	-0.4929
Qx	-1.1501	-0.8215	-1.1501	-0.8215	-0.1643	-0.4929	-0.1643	-0.4929

3.1.3 Pulse Shaping

Pulse Shaping consists on the process of altering the shape of the waveform of transmitted pulses, with the objective of making it better suited to a specific communication channel. Applying pulse shaping can reduce the effective bandwidth required for the transmission, therefore preventing the arise of distortions introduced by the channel, like the intersymbol interference. For the simulation, emphasis was set on two types of pulse shaping: rectangular and raised-cosine filter, with the latter being represented on the following figure 3.3.
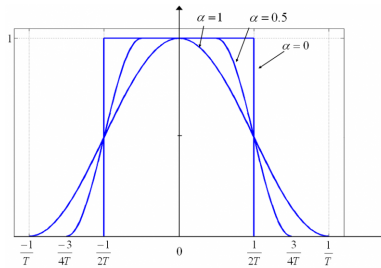

Figure 3.3: Raised Cosine Filter [38]

3.2 Optical System

On the previous section it was discussed how to generate the RF signal. Next it will be described how the different components of the optical signal were modulated in order to simulate the propagation of the signal through the optical system.

The first step on the experimental work was related to the BOSA's transceivers, but modelling it on Matlab would be an hard task to achieve. The objective for the simulation is that the results obtained by it can be compared to the ones captured on the laboratory, and therefore it was chosen to implement the system using external modulation LASER+MZM and to perform the first laboratory experiments using that setup, whose block diagram is depicted in figure 3.4
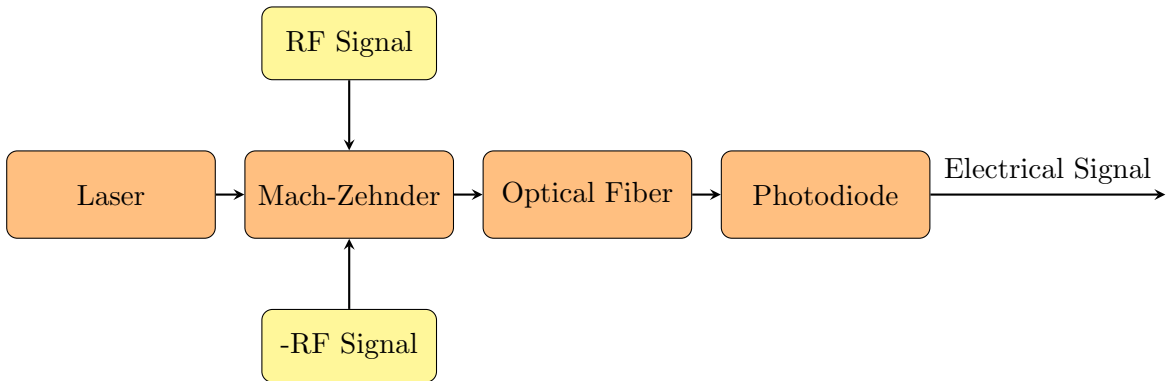
Figure 3.4: Simulation Diagram Block

3.2.1 Laser

The term LASER is an acronym for *Light Amplification by Stimulated Emission of Radiation* and summarizing it consists on the device responsible for emitting light due to the stimulated emission of electromagnetic radiation. Semiconductor LASERs are commonly used in optical transmitters due to their narrow spectral width, high-speed modulation and a satisfactory size. Various types of semiconductor LASERs have been developed, since it's creation, which have improved their performance and reliability, such as the (Fabry-Perot) LASERs, distributed feedback (DFB) lasers, distributed Bragg reflector (DBR) lasers, VCSELs (vertical cavity surface-emitting lasers) and tunable semiconductors lasers in order to improve the performance of optical networks.

Stimulated emission occurs when a photon stimulates the transition of an electron in the conduction band to the valence band and therefore an additional photon is emitted with as much energy and at the same direction as the incident photon.

The type of semiconductor laser considered for the simulation was a single wavelength laser, with the respective characteristics observed in table 3.5 :

Table 3.5: Laser Parameters

Laser Power	0	dBm
Work Frequency	193e12	Hz
Laser Linewidth	100e3	Hz

3.2.2 Mach-Zehnder

As mentioned above the modulator used for the purpose of simulation was a MZM. Next, the formulas used in order to model the MZM are going to be discussed.

The electrical field of a lightwave at the output of a MZM is given by [39]

$$E_{OUT}(t) = \frac{1}{2}\left(e^{j\Delta\Phi_1(t)} + e^{j\Delta\Phi_2(t)}\right)e^{j\omega_c t} \qquad (3.3)$$

Where,
$\Delta\Phi_1$ is the phase change in arm 1.
$\Delta\Phi_2$ is the phase change in arm 2.
ω_c is the optical carrier angular frequency.

The phase changes are obtained by,

$$\Delta\Phi_i(t) = \frac{\pi}{V_\pi}v_i(t), \quad i = 1, 2 \qquad (3.4)$$

With $(\pi/V_\pi) = \eta$ being the index change per volt, V_π the halfway voltage and v_1 and v_2 the voltage signals applied to both arms of the MZM.

On the simulation it was considered the MZM to be biased at quadrature, which means that the operation point is at the centre of the quasi-linear region of the MZM characteristic and therefore offers a maximum of excursion signal, given by the following expression:

$$V_b = (2n-1)\frac{V_\pi}{2}, \quad n = 1, 2, 3, ... \qquad (3.5)$$

Applying tension V_b on arm "1", the phase changes are given by,

$$\begin{cases} \Delta\Phi_1(t) = \eta V_1 sin(\omega_m t) - \frac{\pi}{2} \\ \Delta\Phi_2(t) = \eta V_2 sin(\omega_m t) \end{cases} \qquad (3.6)$$

The main parameters defined for the Mach-Zehnder modulator can be seen on the following table:

Table 3.6: Mach-Zehnder Parameters

$V_{DC_{UP}}$	0	V
$V_{DC_{LOW}}$	0	V
V_{PI}	1	V
Insertion Loss	0	dB

3.2.3 Optical Fiber

Pulse propagation in an optical fiber communication system is described by the non-linear Schrdinger equation (NLSE), on the following manner [40]

$$\frac{\partial A}{\partial z} + \frac{\beta_1 \partial A}{\partial t} - \frac{i}{2}\frac{\beta_2 \partial^2 A}{\partial t^2} + \frac{\alpha}{2}A = -i\alpha_0|A|^2 A. \tag{3.7}$$

Where

A is the pulse envelope in t and in spatial position z.

β_1 is the first order dispersion parameter that causes pulse delay.

β_2 is the second order dispersion parameter which causes pulse broadening due to chromatic dispersion.

α is the attenuation coefficient of the fiber.

α_0 is the non-linearity coefficient of the fiber and it's related to the light strength.

i is a complex vector notation.

Since the type of fiber that is going to be analysed is the Standard Single Mode Fiber (SSMF), modal dispersion will not have to be taken into account and therefore Equation (6.1) can be written as:

$$\frac{\partial A}{\partial z} = -\frac{\alpha}{2}A + \frac{i}{2}\beta_2\frac{\partial^2}{\partial^2} + i\alpha_0|A|^2 A. \tag{3.8}$$

The chosen method to solve Schrodinger was the split-step Fourier Method (SSFM), which divides the fiber into many segments and is therefore able to describe the evolution of the optical envelope in the optical fiber. On the SSFM, nonlinear impairments and dispersion are assumed to act independently over a small step size. The smaller the size of the step is, the more accurate the result becomes, but it has the downgrade of requiring more computational time. In favor of explaining more clearly the SSFM, Equation (6.2) was re-written on the following way:

$$\frac{\partial A}{\partial z} = [\hat{D} + \hat{N}(A)]A. \tag{3.9}$$

Here, $\hat{D}$ and $\hat{N}$ are the operators that account for dispersion and nonlinearity, respectively. The fiber loss can be included on either operators, but for the simulation it was decided to incorporate it with the dispersion operator

$$\hat{D} = -\frac{i}{2}\beta_2\frac{\partial^2}{\partial^2} - \frac{\alpha}{2}, \quad \hat{N}(A) = i\alpha_0|A|^2. \tag{3.10}$$

Going forward it was chosen to select the symmetrical split-step scheme. Employing it, resulted on the approximate solution for the equation (6.2) [41]

$$A(z+h,t) = exp(h\hat{D})exp\left(\int_z^{z+h} \hat{N}(z')dz'\right)A(z,T). \tag{3.11}$$

In retrospective, it would had been more precise to use the asymmetrical split-step scheme, because the computational cost becomes approximately the same, with the increase of steps [41]. The approximation using this method is the following

$$A(z+h,t) = exp(\frac{h}{2}\hat{D})exp\left(\int\limits_{z}^{z+h} \hat{N}(z')dz'\right) \frac{h}{2}A(z,T).$$ (3.12)

Whence, in order for simulating propagation of RF signal on the optical single mode fiber, equation (6.5) was implemented, and the fiber was created with these specific values for the parameters:

Table 3.7: Single Mode Fiber Parameters

Dispersion	17	$\frac{ps}{nm \times km}$
2nd Order Dispersion	17	$\frac{ps}{nm \times km}$
3rd Order Dispersion	0.55	$\frac{ps}{nm \times km}$
Loss Coeficient	0.22	$\frac{dB}{Km}$

3.2.4   Photodiode

Photodiode, which are one of the most popular sensor types for light-based measurements, are responsible for converting the signal from optical to electrical. The photodiode generates a current proportional to the light that it receives, and then converts it to a certain output voltage. Therefore a photodiode, simply said, corresponds to nothing else other than a transimpedance amplifier circuit.
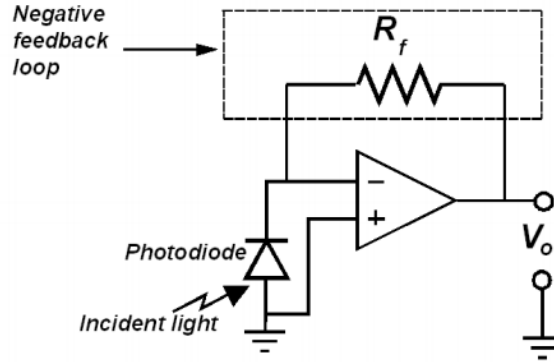
Figure 3.5: PIN internal structure [42]

The equation used to model the photodiode was nothing else than the Ohm equation:

$$V_{out} = I_{in} \times R_f$$ (3.13)

The photodiode during the process of conversion from optical to electrical adds noise to the system. For the simulation purpose a noise floor was added to the system at this stage, in order to rightfully implement the limitations that come from a real system. The noise value has to be tuned in order for the system to have the SNR that presents results closer to

the ones expected. The following matlab code is responsible for the implementation of the guassian white noise on the signal,

```
1  % Desired SNR
2  snr_db = 22;
3  Signal = awgn(Signal,snr_db,'measured');
```
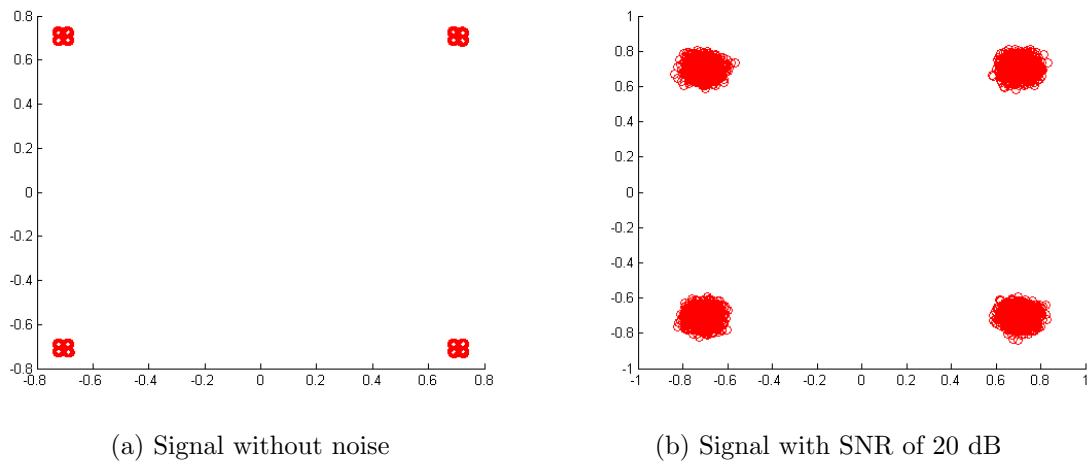

(a) Signal without noise

(b) Signal with SNR of 20 dB

Figure 3.6: Received Constellation: Noise effect

3.3   Considerations

The Nyquist Sampling Theorem states that if a continuous-time signal is periodically sampled at a rate of at least twice of the highest-frequency sinusoidal component contained within the signal, than it's possible to recover perfectly the original time-varying signal from the periodic samples.

The process of sampling an analogue signal is explained by the relation [43],

$$x(n) = x_a(nT), \quad -\infty < n < \infty \tag{3.14}$$

where x(n) is the discrete-time signal obtained by the fact that every T seconds there is a sample taken of the analogue signal $x_a(t)$. The relationship between the time variable of continuous-time and n of discrete-time signals, is related with the following expression, and the process can be observed in 3.7

$$t = nT = \frac{n}{F_s} \tag{3.15}$$
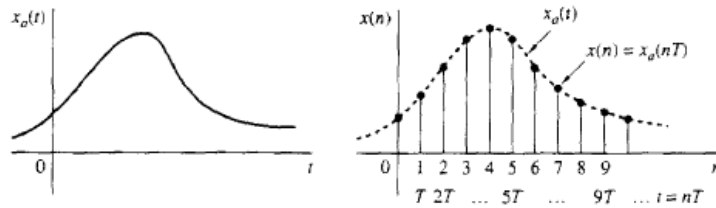
Figure 3.7: Periodic Sampling of an Analog Signal [43]

The problem is that by sampling the same discrete-time signal, an infinite number of continuous-time sinusoids can be represented, which is responsible for an ambiguity on what continuous-time signal, $x_a(t)$ is actually represented by $x(n)$. On the other hand, if explained from the frequency perspective, it's equal to saying that sampling a certain signal, with frequency F_0, with a rate of F_s, will lead to the following infinite group of frequencies that will be indistinguishable from the original frequency,

$$F_k = F_0 + kF_s, \quad -\infty < k < \infty \tag{3.16}$$

Those frequencies are denominated of aliase of F_0, and an example is showcased in 3.8,
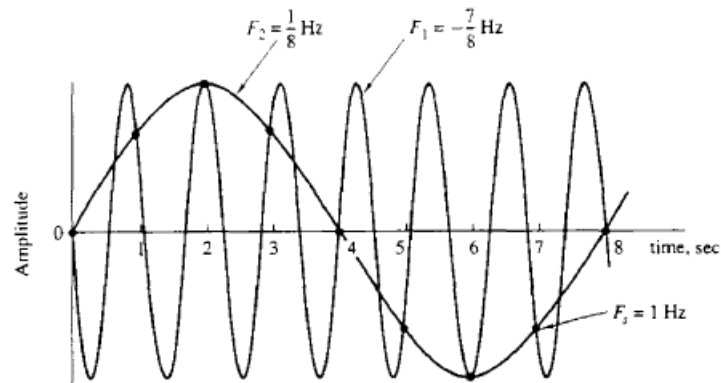
Figure 3.8: Example of Aliase Frequencies [43]

Concluding, when designing a sampling system, the following considerations are required, [44]:

☐ Determining the highest frequency sinusoid that is presented on the analog input signal;

☐ Determine the minimum ammount of guardband that can be colocated;

☐ Based on the previous two points, calculate the Sampling Rate using the following equation

$$F_S = 2F_0 + guardband \tag{3.17}$$

Due to the nature of real low-pass filters, having an wider guardband range will make the reconstructed output power more accurate, but it has the disadvantage of increasing the complexity of the system with an higher sampling rate.

3.4 Reception

After the signal has propagated through the optical system and been received by the photo-detector, the processes that were made in order to convert the stream of bits into an RF signal, will have to be performed on the reverse order to convert the RF signal into the corresponding stream of bits. Comparing the conditions onto which the signal was received with the generated signal is required in order to have a measure of the performance of the system. On figure 3.9, the block diagram for the reception process, with the several steps, is shown.
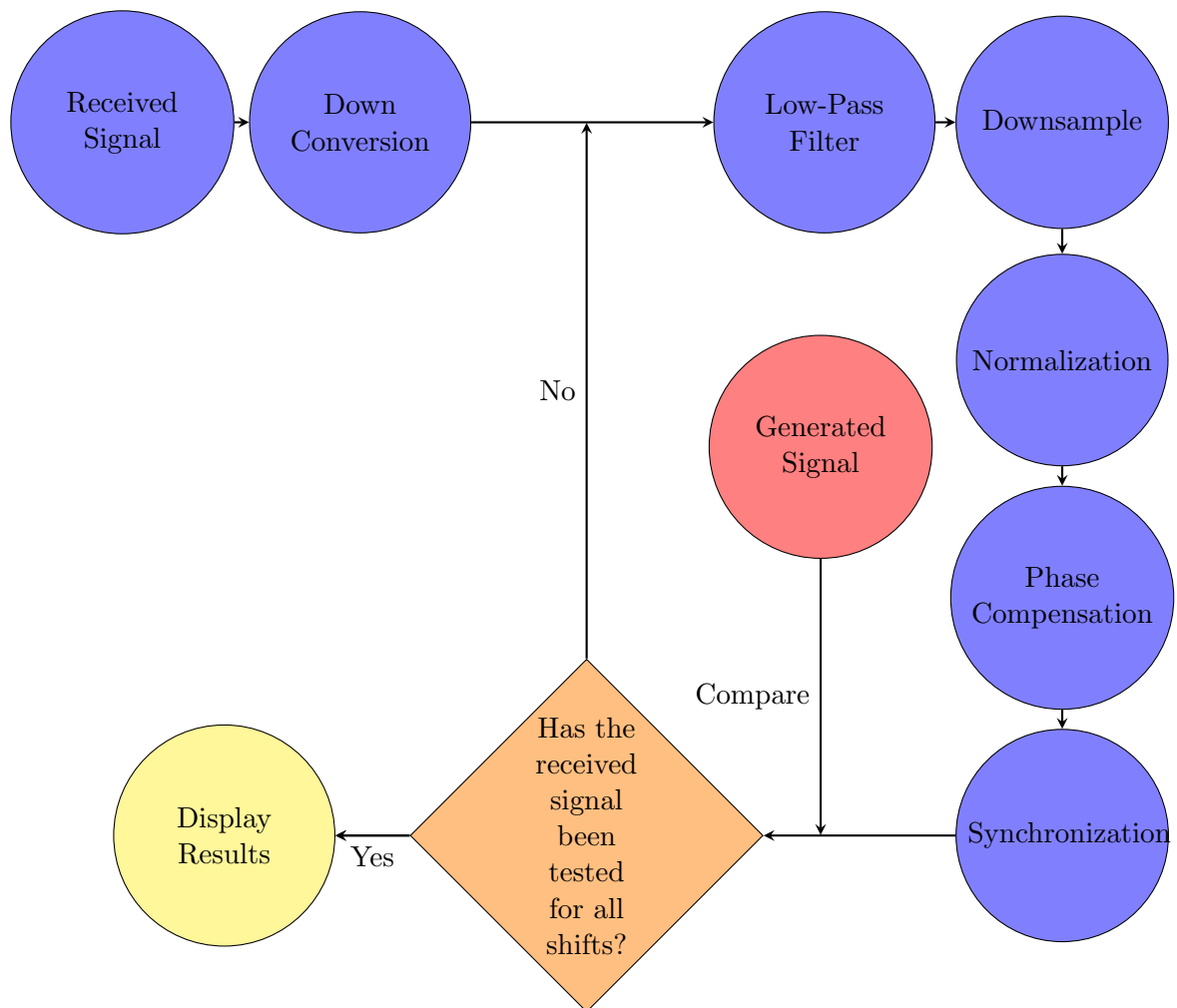
Figure 3.9: Reception Diagram Block

The first process consists on establishing the signal to baseband. After, the baseband conversion, the signal will go through a low-pass filter in order to cut the undesired frequencies. The low-pass filter implemented type was a besself with an order of 4 and a bandwidth which varied based on the symbol rate of the signal.

The process described above can be observed on 3.10.

The spectrum of the received signals are the following:
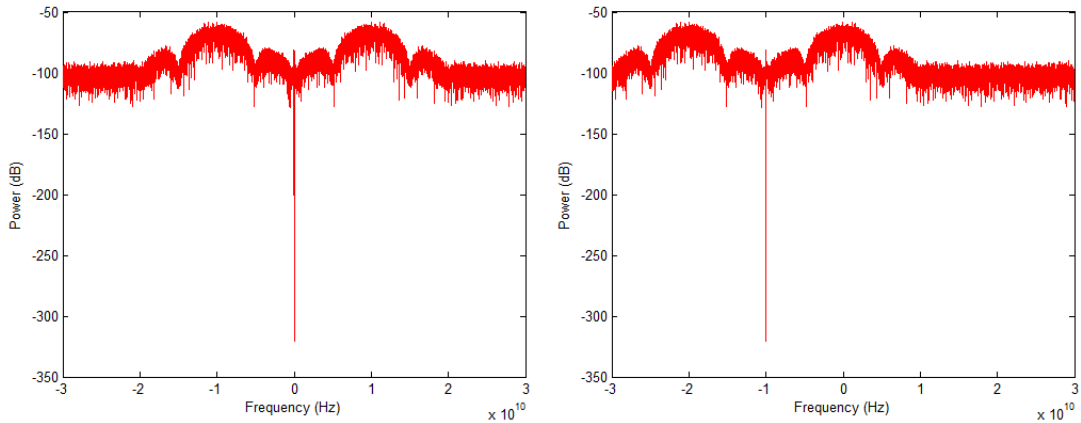
(a) Received Spectrum Signal

(b) Received Signal after down-conversion
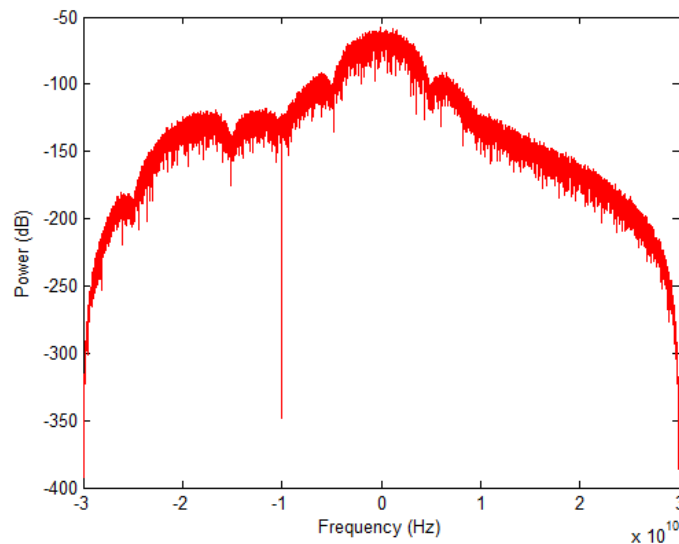
(c) Baseband Signal I/Q after low-pass filter

Figure 3.10: Received Constellation: Noise effect

Choosing the right starting sample to initiate the down-sample process is of great importance, because depending on the chosen sample, the received signal can either keep or loose the original properties that it possessed. Getting the right sample becomes an easier task with the increase of the sample rate, because the best sample is the one located at the middle of the symbol and with the increase of the number of samples per symbol, it's more likely that there will exist a sample close to that point, making possible to recover the signal to its original state. If the sample rate isn't relatively high compared to the data rate, and therefore there are few samples per symbol, the process of interpolation can be a solution, which actually ended being applied for these situations.

The following step consists on performing the normalization of the signal. Later on this section, it will be explained how the different modulation formats were implemented and

where the symbols were allocated. But normalization of the signal happens so the signal respects the implementation of normalized constellation for the varied modulation formats and therefore respected the position where the decision is performed, so that it is guaranteed that the symbol is being coded with the right combination of bits.

```matlab
1  % Normalizing the received signal
2  sig_abs = abs(sig);
3  sig = sig/mean(sig_abs);
4  sig = sig - mean(sig);
```

In the following figure, it's possible to visualize an example where the signal received is not normalized. After the implementation of the normalizing code,

(a) Not normalized constellation signal

(b) Normalized constellation signal
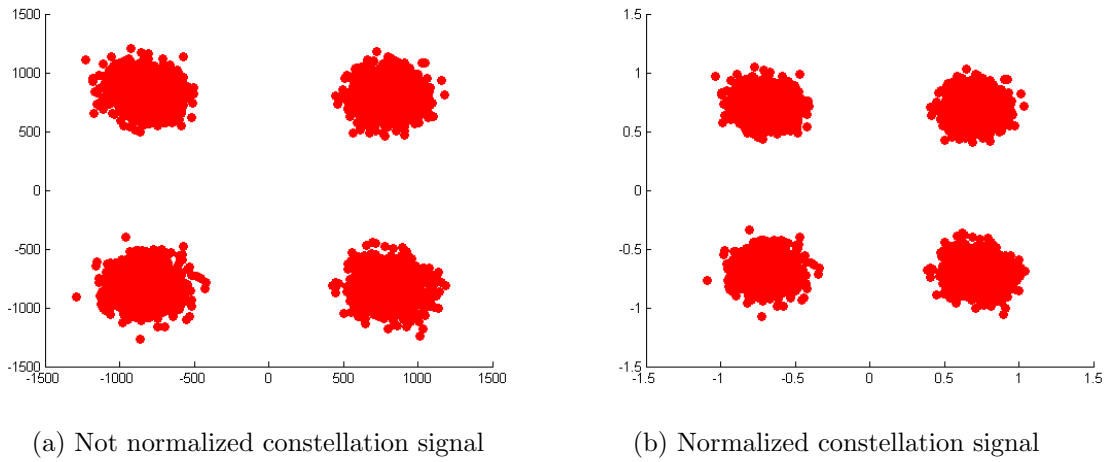
The phase compensation block is particularly of interest for the experimental work, due to the fact that the signals retrieved from the oscilloscope have a phase shift, which is needed to remove, so it's possible to receive the information that was sent. That is, if the system is working correctly.

The following algorithms will give the angle shift value, that it's needed to apply on the signal, so the signal has no angle on both real and imaginary component.

For the QPSK and 16-QAM modulation formats, that angle shift is given by the expression 3.18,

$$\theta_{QPSK,16-QAM,64-QAM} = \frac{1}{4}\left(\frac{1}{N}\sum_{i=0}^{N-1} signal_i^4\right) \tag{3.18}$$

But since on the QPSK and M-QAM modulation formats, the symbols are located with a phase shift of $\frac{\pi}{4}$, that has to be added to the value obtained from equation 3.18.
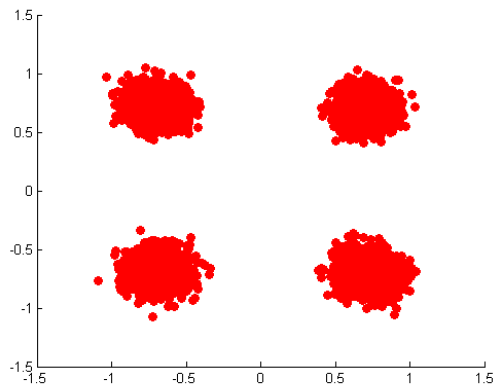
$$signal = signal \times e^{(-j(\theta+\frac{\pi}{4}))} \tag{3.19}$$
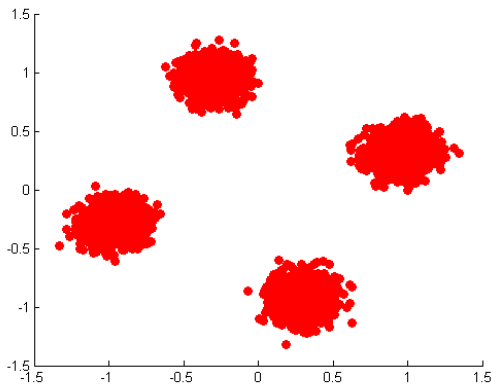
(a) Constellation from received signal
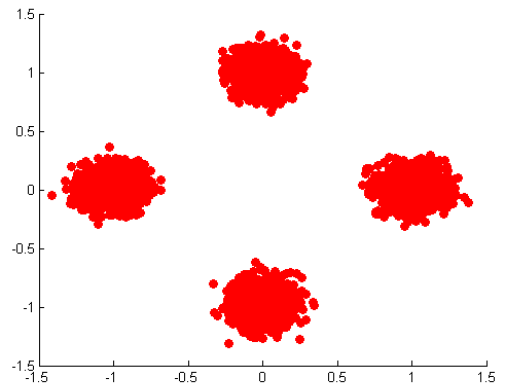
(b) Constellation after removing phase

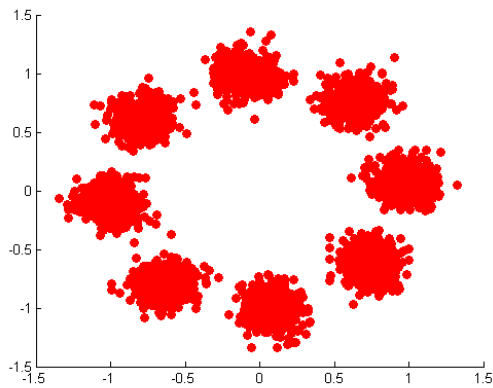(c) Constellation after all compensation algorithm

Figure 3.12: Signal Constellation before and after the phase compensation algorithm

To compensate the phase shift on the signals received modulated with 8-PSK, the expression 3.20, was used,
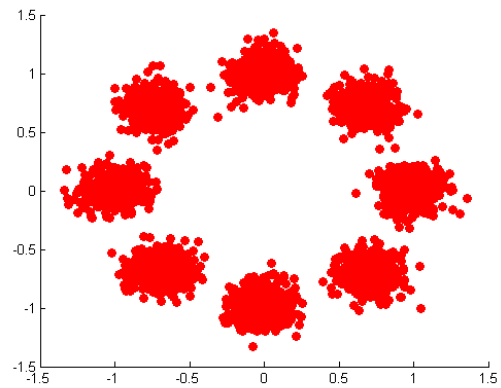
$$\theta_{8PSK} = \frac{1}{8}\left(\frac{1}{N}\sum_{i=0}^{N-1} signal_i^8\right) \tag{3.20}$$

$$signal = signal \times e^{-j\theta} \tag{3.21}$$

From observing 3.21 it's possible to observe that contrary to the other modulation formats, for 8-PSK modulation format, the compensation algorithm doesn't need to have an extra component added to the angle obtained by equation 3.20.

(a) Constellation before algorithm

(b) Constellation after algorithm

Another problem that arises is related to the synchronization between the generated and received signal. With the signals synchronized it is possible to conclude how many bit errors occurred by comparing both vectors and checking for the differences, where the number of different bits will give the amount of error values. But how exactly can you align the signals for them to be synchronized? The answer is by the process of *cross-correlation*.

Cross-correlation returns the measure of similarity between both signals as a function of the lag of one relative to the other. Obtaining the peak of this function will give you the position where the signals share the most similarities, which on our specific case.The following code on MATLAB is the process followed to obtain the plot of the cross-correlation between the generated and received bits stream,

```
1  % Obtain the cross-correlation between the Generated and Received signal
2  [C1,lag1] = xcorr(data_received,data_generated);
3
4  figure()
5  plot(C1);
```

The behaviour observed on figure 3.14, shows an example of two signals, both with a dimension of 10^4 which are synchronized at the location where the maximum happens. The code shown bellow is responsible of converting the index where the maximum of the cross-correlation happens, with the point that will pronounce how the concatenation of the new vector will be done.

```
1   %Finding the position where the max occurrs
2   [maximum,index] = max(C1);
3
4   %Transforming the index into the respective synchronization sample position
5   index = rem(index,(nBits*2));
6   SampleDiff = index−nBits;
```

The value obtained for the sample by the algorithm implemented, can either be negative or positive and based on that, the concatenation of the generated vector will be different. After the concatenation is performed, the generated bit vector will therefore be synchronized with the received bit vector error.
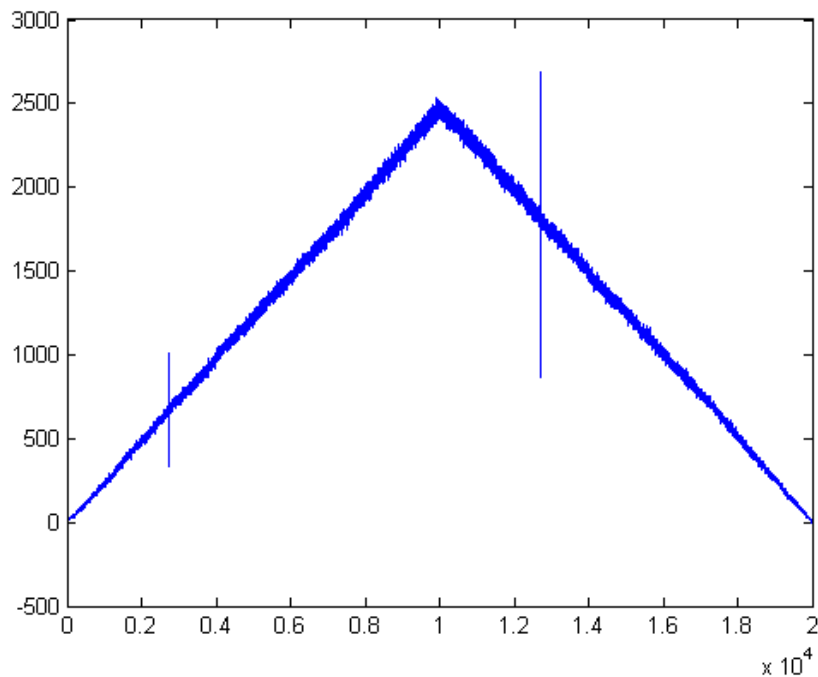
Figure 3.14: Cross Correlation obtained for generated and received bits stream

As it was already mentioned, on previous blocks, treatment was implemented on the signal not only to regulate it's phase, but also to normalize it. Looking to the appearance of the received signal, everything would seem to be working according to expected, but the problem arises when we take notice that the phase shift compensation code, works only, as a method to align the signal symbols to an angle where the constellation has apparently the same appearance as the original constellation, but the same might not be said about the symbols.

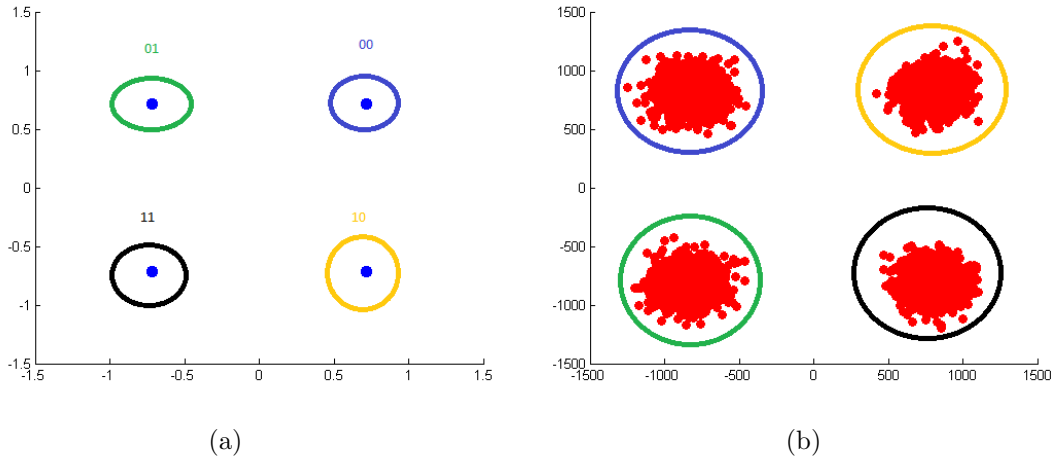(a)   (b)

Figure 3.15: Phase Shift observed on the QPSK modulation format

The results observed on 3.15b are a possibility, with the phase algorithm implemented, because of chromatic dispersion. As it can be observed, on this situation, the phase algorithm set the constellation to the desired appearance, but the generated symbols will not be retrieved with the same information. For example the generated symbol that corresponded to the combination '00' will now be recovered as '01', which alone basically ruins the performance of the system. But the same happens to the other symbols.

Considering that the system isn't affected by highly non-linear phenomenon, for the quadratic modulation formats, the phase shifts implemented on the signal were multiple of $\frac{\pi}{4}$,

$$phase_{shift} = \left[0, \frac{\pi}{4}, \frac{\pi}{2}, \frac{3\pi}{4}\right] \tag{3.22}$$

While for the 8-PSK modulation format, the phase shift angles simulated were the following,

$$phase_{shift} = \left[0, \frac{\pi}{8}, \frac{\pi}{4}, \frac{3\pi}{8}, \frac{\pi}{2}, \frac{5\pi}{8}, \frac{6\pi}{8}, \frac{7\pi}{8}\right] \tag{3.23}$$

The principle consists on performing a loop where the received signal is manipulated with the various angles, so all possibilities are tested out. When the loop is concluded, analysing the results obtained for all the shifts will make it possible to know for what shift the signal was correctly synchronized.

3.5 Evaluation Metrics

In order to draw a comparison between the transmitted and received RoF signal, the metrics selected were the Bit Error Rate (BER) and the Error Vector Magnitude (EVM). BER is one of the most popular criteria for assessing the performance of communication systems and basically what it indicates are the number of bit errors divided by the total of transmitted bits during a certain studied interval.

$$BER = \frac{n \; bits \; errors}{n \; total \; bits \; transmitted} \tag{3.24}$$

The *EVM* is the effective distance between the received complex symbol and it's ideal location on the constellation diagram [45].
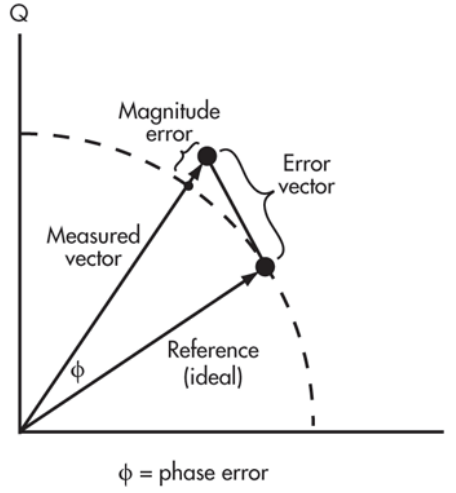
Figure 3.16: EVM Calculation Method [46]

It is defined as RMS of the difference between measured and ideal symbols, normalized with the average symbol energy, as it can be seen of the following expression:

$$EVM_{RMS} = \sqrt{\frac{\frac{1}{N}\sum_{n=1}^{N}|S_r(n) - S_t(n)|^2}{P_0}} \tag{3.25}$$

Where
N is the number of symbols.
$S_r(n)$ is the transmitted values of the nth symbol.
$S_t(n)$ is the received values of the nth symbol.
P_0 is the average power of the all constellation symbols.

If the modulation format used corresponds to a quadratic constellation, it's possible to relate EVM and BER, by the approximation [47]

$$BER \approx \frac{(1 - L^{-1})}{log_2 L} erfc[\sqrt{\frac{3log_2 L}{(L^2 - 1)}\frac{\sqrt{2}}{(kEVM_m)^2 log_2 M}}] \tag{3.26}$$

43

On this estimation, L corresponds to the number of identical signal levels within each dimension of the constellation and log_2M as the number of bits encoded into each of the QAM signals. The EVM has an advantage upon BER, which is the fact that it gives a measure of the wanted performance before the demodulation process. [48].

3.6 Simulations Results

With everything that has been mentioned above regarding the implementation of the generation and reception of the RF signal, on this section the results given by the simulation platform are going to be shown next and analysed.

3.6.1 Signal Generated

On the following sub-plots it's possible to first observe the baseband spectrum of the generated signal and then the respective constellation. The generation of the signal was used by recurring to rectangular up-sampling and a sample rate of 60 GHz.

(a) QPSK baseband spectrum

(b) 16-QAM baseband spectrumn

(c) 8-PSK baseband spectrum

(d) 64-QAM baseband spectrum
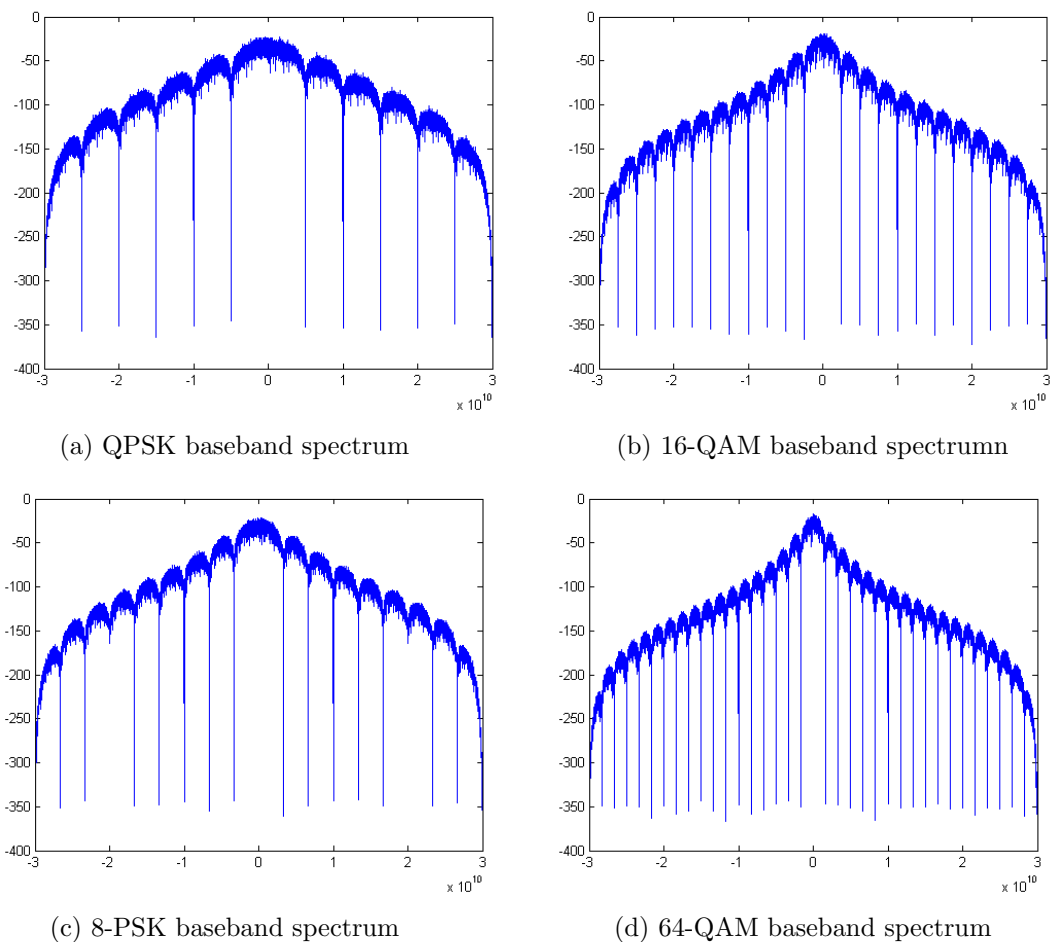
Figure 3.17: Baseband Spectrum for the different modulations formats using rectangular pulse-shaping
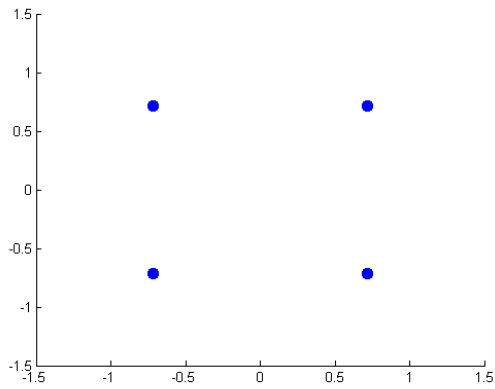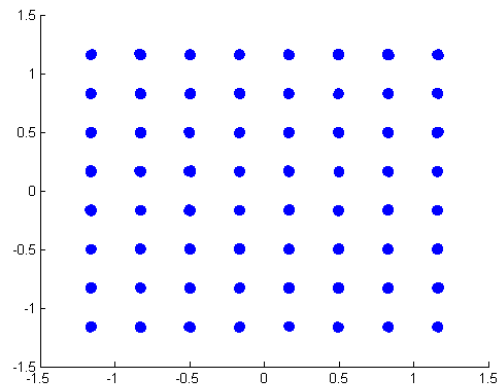
(a) QPSK constellation
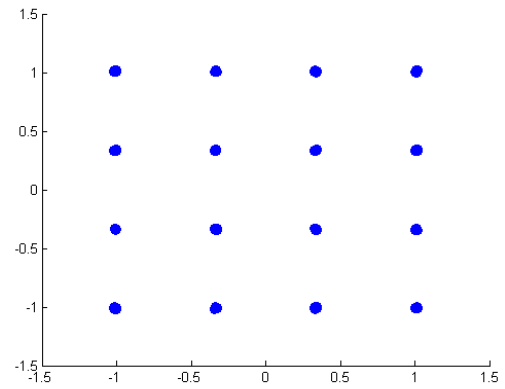
(b) 16-QAM constellation
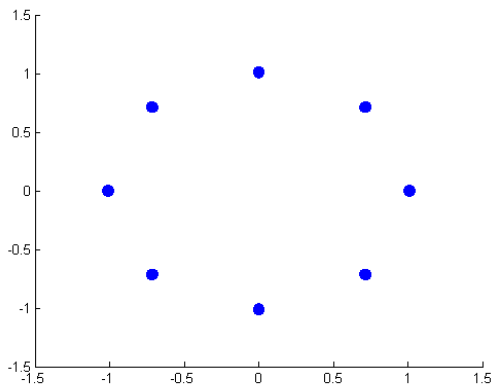
(c) 8-PSK constellation

(d) 64-QAM constellation

Figure 3.18: Generated Constellations for the different modulations formats

3.6.2 Simulation I - System without noise

On this subsection it's possible to observe the first simulation performed, which was done without the introduction of any noise in the system, particularly, at the photodiode which is the noise source of the system.
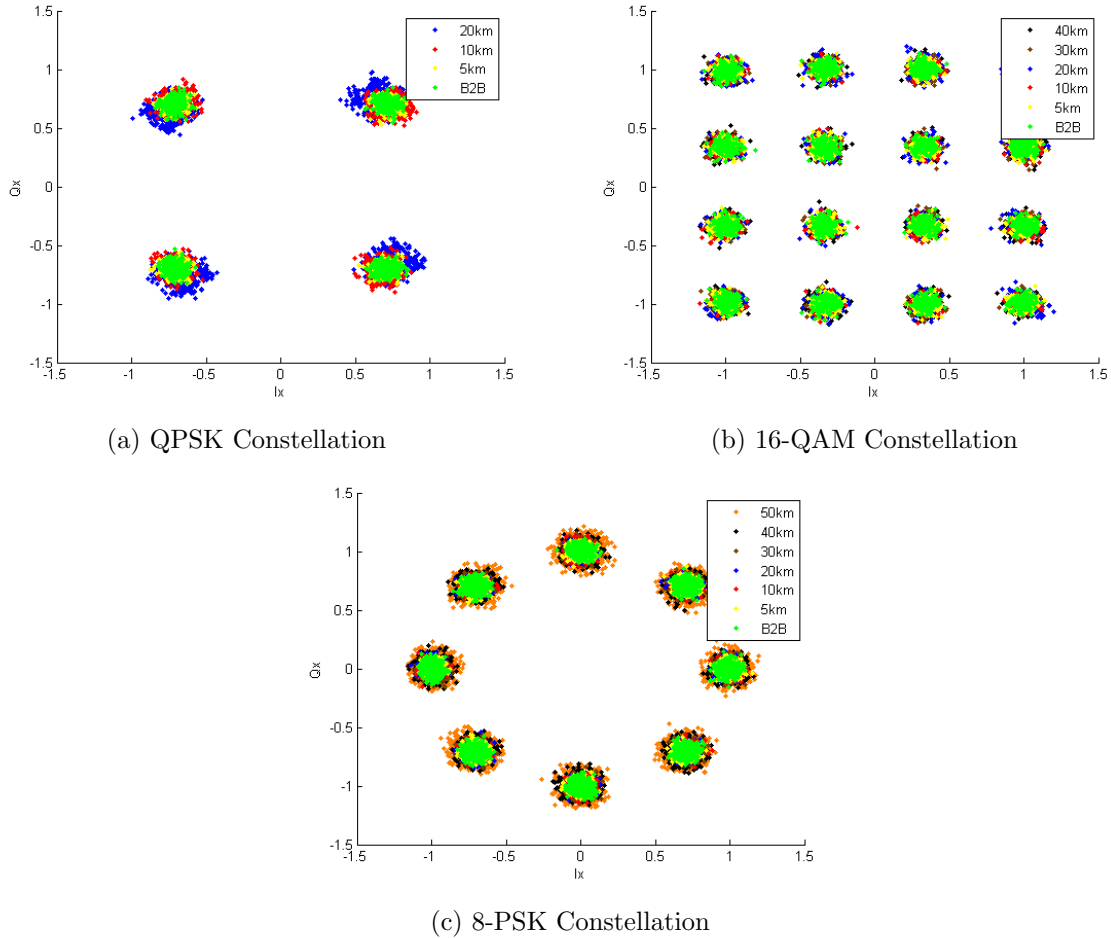

(a) QPSK Constellation

(b) 16-QAM Constellation

(c) 8-PSK Constellation

Figure 3.19: Impact of the chromatic dispersion on the constellation for several fiber lengths

3.6.3 Simulation II - System with fixed SNR

The first set of results consist on the propagation of the RF signal, mapped with different modulation formats, on several fiber lengths. But for this set of simulations, the photodiode was modelled to always generate, independently of the power of the signal, an electrical signal with a SNR of 22 dB. This condition allows to focus primarily on the impact of the chromatic dispersion on the performance of the optical pulse.

The fact that the RF signal is double sideband, the effect of chromatic dispersion will not be as linear as it is for the single sideband signals, and therefore it is of importance to analyse the impact of chromatic dispersion not only based on the modulation format chosen but also for the fiber length of the optical system selected.
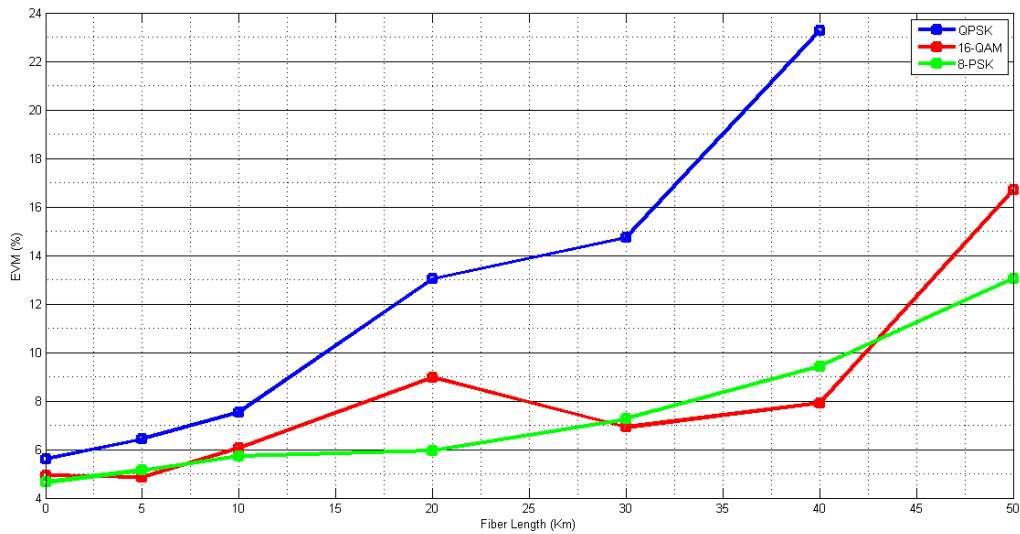
Figure 3.20: Graphic of EVM vs Fiber, for a received signal with the same SNR independently of the optical power

By analysing the graphics, its obvious that QPSK is the one which presented the worst results, since with the increase of the fiber length, the difference in EVM comparing to the other modulation formats studied kept increasing.

Table 3.8: Symbol Rate for the different modulation formats for a bit rate of 10Gbit/s

QPSK	5	Gbaud/s
16-QAM	2.5	Gbaud/s
8-PSK	≈ 3.3	Gbaud/s

The explanation for this behaviour consists on the fact that the velocity onto which the symbols are being propagated,on the QPSK, is the highest and consequently the distance between each symbol is the lowest, as it can be seen on table 3.8, which causes the signal to be more sensitive to pulse spreading due to the chromatic dispersion. A signal affected by intersymbol interference will therefore become more noisy and become less reliable. The advantage for the QPSK, consists on the fact that even though it might suffer more due to chromatic dispersion, it has an higher tolerance to the deviation provoked by it, due to the inherent conditions of its constellation, therefore even though it might present an higher EVM than the other modulation formats, it won't translate into as many bit errors.

Regarding 16-QAM and 8-PSK, it seems that at least for most of the fiber length dimensions measured, the behaviour of the 16-QAM was relatively worse than 8-PSK, which was a bit of expect due to the fact that even though 16-QAM presents a lower symbol rate, it has a lot less tolerance than 8-PSK to degradation of the signal. Using the line of thought mentioned above the fact that for 16-QAM the symbol rate is lower would be an advantage over 8-PSK, but comparing its possible to notice that the difference isn't that considerable.

Explaining this, the incertitude on the precision of the simulated system is not the main focus point, but the fact that the signal being studied is double sideband. Chromatic dispersion is responsible for the propagation of both bands on different velocities, which at some fiber lengths the impact can be completely ruinous for the signal and therefore it is affected by the modulation format chosen, due to the correspondent spectral width of the signal.

3.6.4 Simulation III - Mixed effect of dispersion and attenuation

The settings for the second simulation done, forced that the only reason why the performance of the system would deviate would be only up to chromatic dispersion, since the effects of attenuation were not being taken into the account, since a static SNR was fixed on the system, independently of the power of the signal.

On this next simulation, the system has a noise floor value, which is added by the photodiode. That noise floor will degrade more the signal with the decrease of it's power and each point that can be see on the plots, was obtained by the simulation and analysis of half a million points, which can definitely give the system a decent precision on the results.
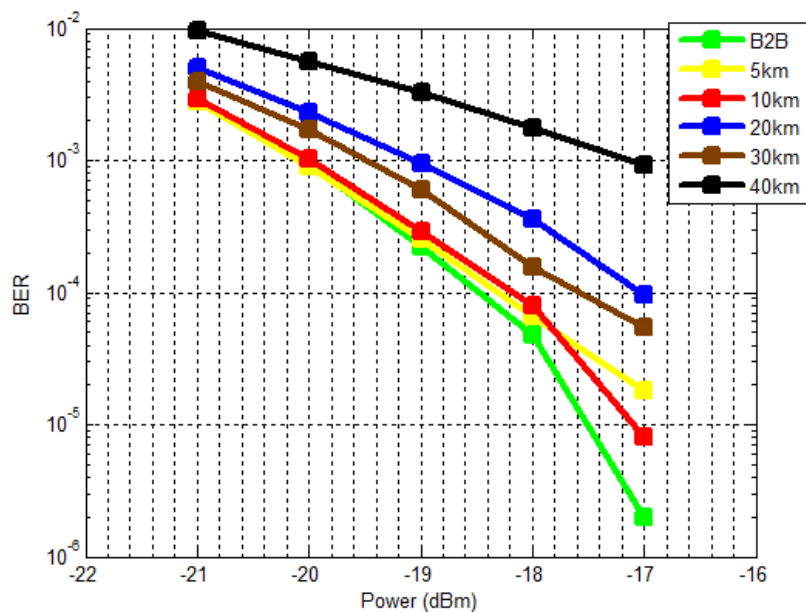

Figure 3.21: QPSK modulation BER vs Power graphic

Observing 3.21 its possible to conclude that the results obtained for the situations of B2B, 5 km and 10 km fiber, show almost the same behaviour. The conclusion which can be brought is that for these specific fiber lengths the system has yet to feel a significant impact from chromatic dispersion.

For the other fiber lengths it's possible to visualize a clear power penalty on the system, caused by chromatic dispersion. However the surprise comes for the fact that the performance for the 30 km fiber is actually better than it is for 20 km of fiber.
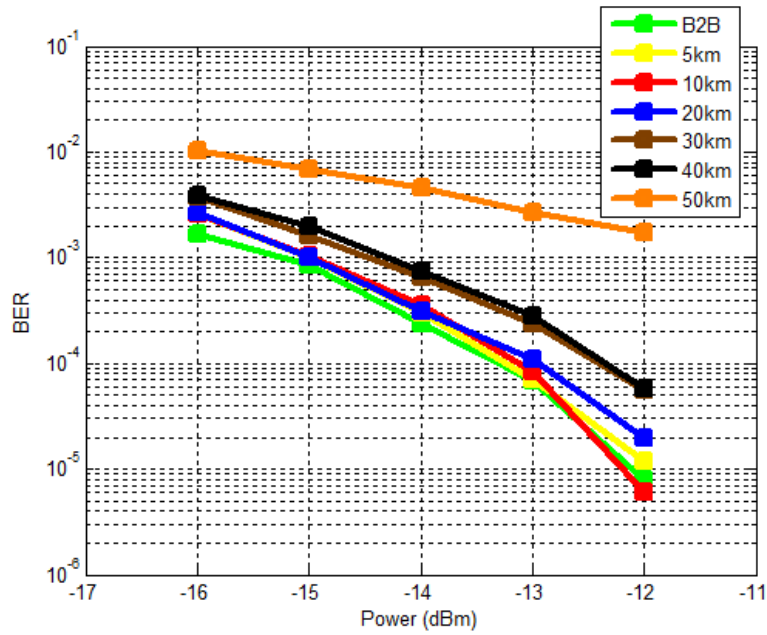
Figure 3.22: 8-PSK modulation format BER vs Power graphic (SNR = 30dB)

On this new measures the results were obtained when the SNR introduced was of 30 dB,
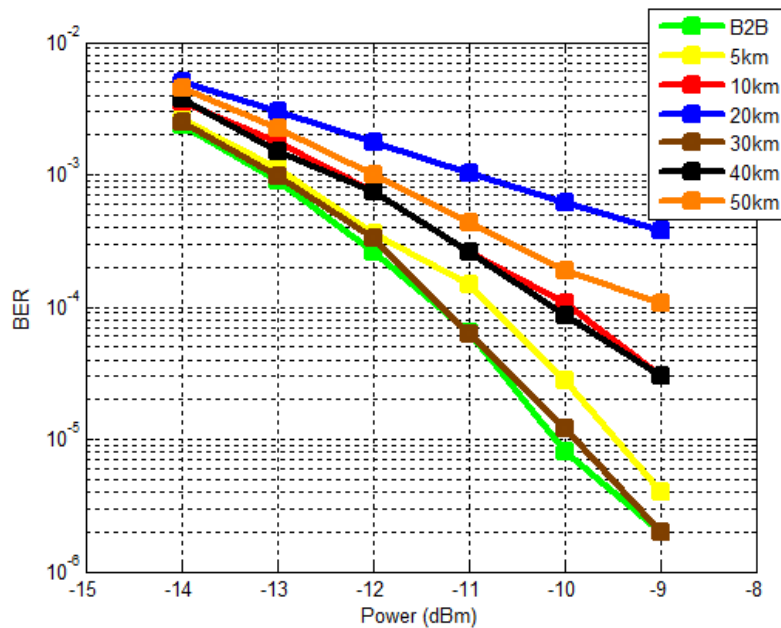

Figure 3.23: 16-QAM modulation format BER vs Power graphic

Now that the graphic for the QPSK has been evaluated, it is the moment of interpret the results obtained for 8-PSK and 16-QAM, respectively figures 3.22 and 3.23. For the 8-PSK situation, as it had been the case for the QPSK's, the performance of the system doesn't seem to be affected by the introduction of by the first kilometers, though at this situation the 20

km case is included. Comparing the sensivity between the 8-PSK and QPSK, as expected the results are worse for the 8-PSK, because the toleration of the QPSK's constellation is a lot higher than it is for the 8-PSK, since even if the QPSK has an higher EVM, for most of the possible cases it will traduce still into a lower BER.

For last it's time to observe the 16-QAM simulation. Compared to the previous ones, this ones is the one who shows the most unexpected behaviour of all, since for example the results obtained for the transmission of the RoF signal through 30 km of fiber is giving a closer performance to the one that is obtained both to B2B and 5 km. For this situation the system shows the worst performance out of all when the fiber block has a length of 20 km.

Following the line of thought that was made to analyse the difference in the sensibility obtained for the different BER values, the explanation is done to show why 16-QAM has the worst sensitivity out of the three.

Back in section 2.8.2, a phenomenon denominated of power degradation was mentioned, since based on some of the literature found, it is a consequence of the chromatic dispersion on double sideband signals. Depending on the carrier frequency used and the respective fiber length, the effect of the chromatic dispersion will vary and it might explain the behaviour it's observed on 3.20.For the frequency carrier of 10GHz, case of the signals simulated, the first power cancellation happens around the 36 Km and then it repeats every 72 Km, approximately.
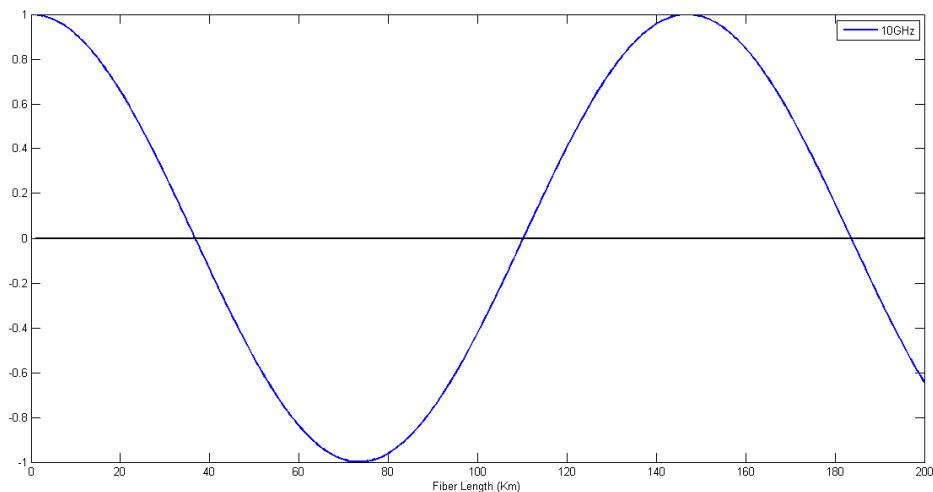

Figure 3.24: RF Power of the generated Radio Frequency

However based on these values, no correlation was possible of achieving between the occurrence of this phenomenon of power cancellation for the characteristics of the RF carrier with the graphics that were obtained above.

3.6.5 State of the simulation results - backup previous results

So far, the justification for the results that have been observed has been attributed to the chromatic dispersion, because of the negative effect it has on the propagation of double sideband signals. Even if it hasn't been possible to completely trace the behaviour and the impact provoked by it, it is crystal clear that the performance depends manly on three parameters, which are, the carrier frequency, baud rate and the fiber length. For this last simulation, the only characteristic which was different out of those three, was the baud rate, which associated with the intrinsic characteristics of each modulation format, explains why the chromatic dispersion leads to those results. But in order to verify the truthfulness of the results obtained for the simulation, the system was simulated for a conjunct of conditions, for which the results that should be observed are known.

- The first debug simulation consisted on setting the dispersion parameter to zero, fix the SNR of the system to a static relation and observe the result when the system had to go through hundreds of kilometers. The constellation received had not suffered any effects when compared to the one which was generated, as it is possible to observe on the following figure

- The second condition consisted on studying the system for a low frequency carrier ($F_c = 1.5GHz$), a data rate of 312.5 Mbit/s and finally QPSK as modulation format.The system was simulated for a fiber length of 1000 km and the constellation observed showed no sign of have been affected by dispersion, just as it was expected.

Both these results, give more plausibility to verify the authenticity of the results obtained with the simulation platform.
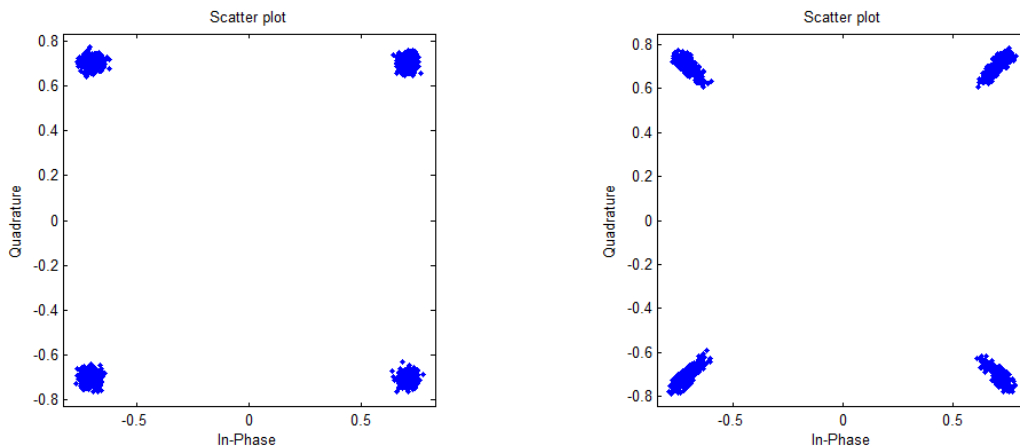
(a) Constellation obtained for the first item situation

(b) Constellation obtained for the second item situation

Figure 3.25: Debug of the veracity of the simulations results by analysing two situations, for which the result is known

3.6.6 Simulation IV - Fixate the baud rate and vary the carrier frequency

In subsection 3.6.4, the system was studied for several fiber length and three different baud rate, due to the distinct modulation formats implemented, with the carrier frequency fixed. Now it was set both the fiber length and the baud rate has fixed parameters, and only the frequency carrier will vary.

With this said, it was decided to fixate the baud rate of the system at 1.25 Gsymbols/s, using QPSK as the modulation format and varying the frequency carrier, to see for which frequency carrier of the RF signal the signal starts to performing worse, as until now none of the simulations had focused on the variation of the RF carrier frequency. However, independently of the attenuation that the signal would suffer due to the propagation through the fiber, the SNR was kept fixed.

The plot that can be visualized at 3.26 and it shows the impact that chromatic dispersion has on the system for a fiber length dimension of 200 km.
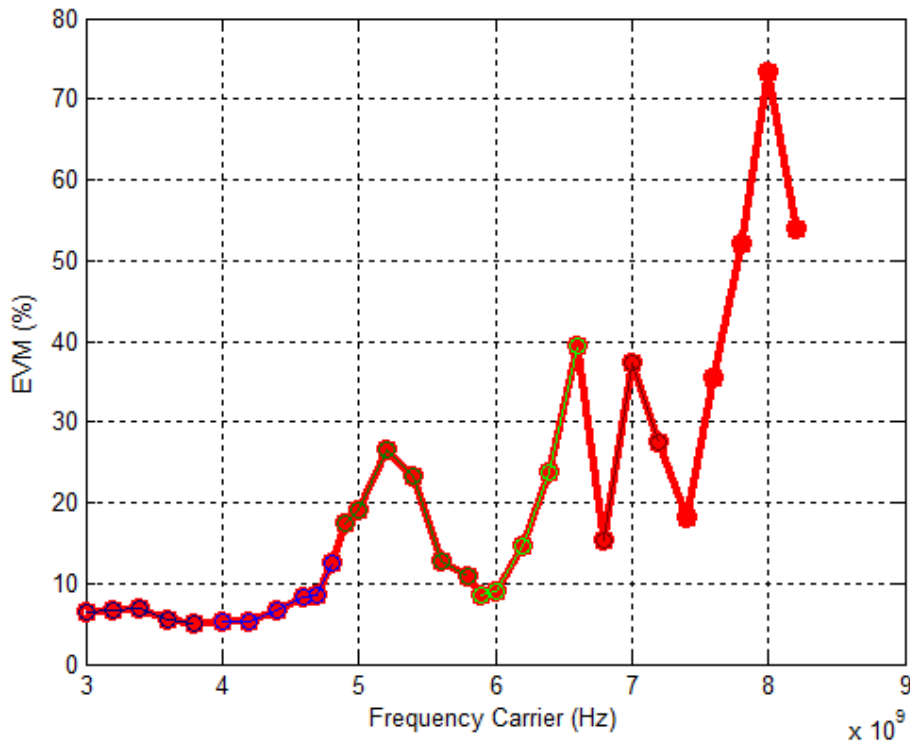

Figure 3.26: Relation between the EVM obtained and the RF frequency, for fiber length of 200 km

As it is possible to observe from the graphic, for the conditions mentioned previously, the EVM shows a pattern similar to a cosine function, since following an increase of EVM, there is observed a decreased for an higher carrier frequency, though overall the function still shows a positive inclination.

(a) Constellation for F_c of 4GHz

(b) Constellation for F_c of 8GHz

(c) Received Spectrum for F_c of 4 GHz

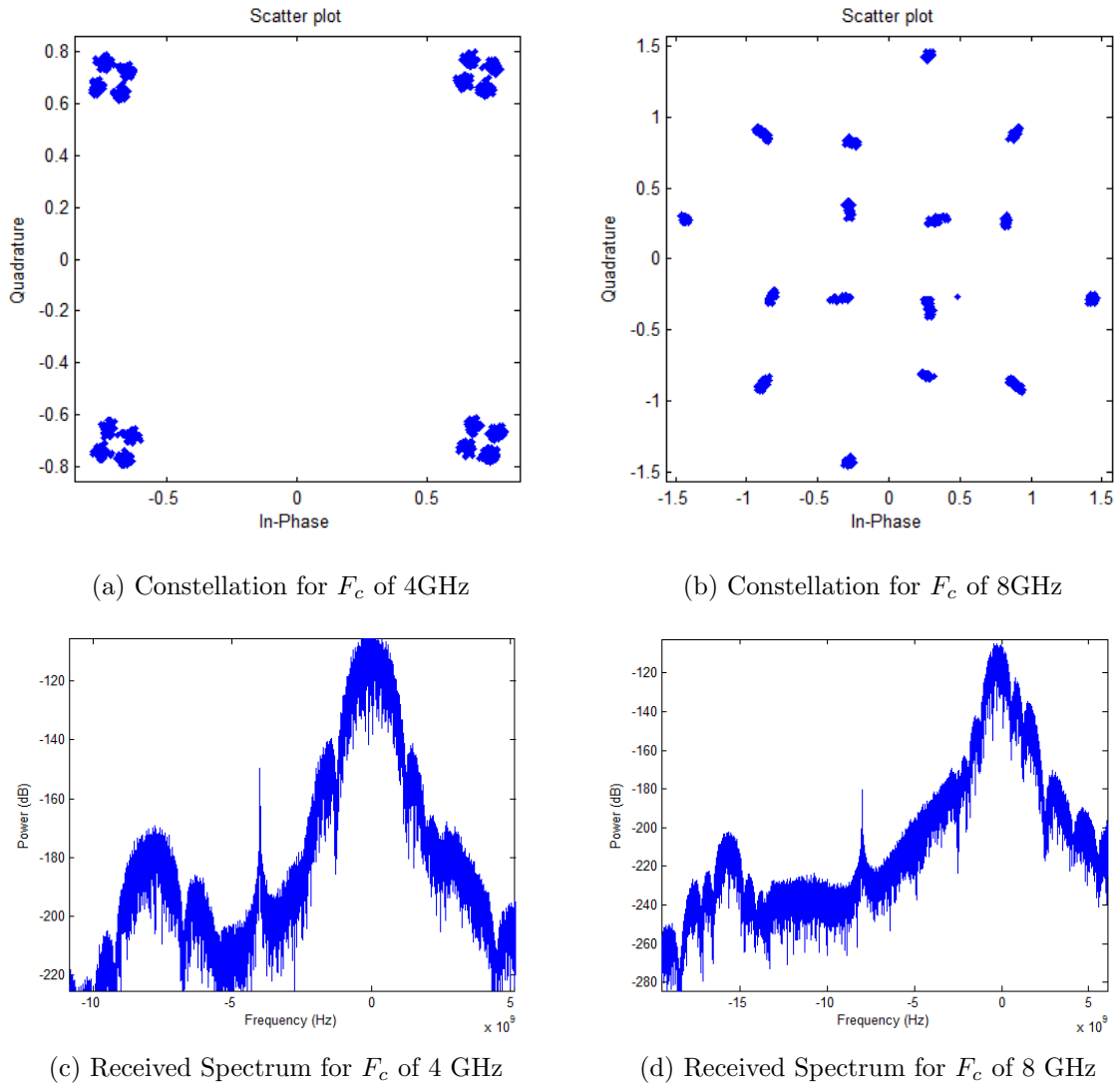(d) Received Spectrum for F_c of 8 GHz

Figure 3.27: Results obtained with fiber length defined of 200 km and a baud rate of 1.25 Gsymbols/s

In 3.27 it's possible to observe the extreme situations obtained on the frequency carrier sweep that was done in 3.26. By comparing both situations, by looking at the constellation plot it's possible to observe that at both situations the effect of dispersion is already noticeable, but however for the 8 GHz case the effect is a lot dire, just as it could had been presumed for the immensely high EVM that was obtained for it.

But looking at the spectrum of both received signals in baseband, it's possible to observe that the low-pass filter successfully attenuated significantly the negative band, and also a dc component that could be observed on the spectrum. The main problem is when we take a look into the lobes next to the primary, since for the 8 GHz situation, it's possible to observe a secondary lobe, which has appeared with a level of power above what was desired, which might explain the results obtained for these situation. Nevertheless, this situation is explained by chromatic dispersion, because of the negative effect it has on each band during

their propagation through the fiber and which leads to problems when the received signal is down-converted.

3.6.7   Results Conclusion

The results obtained from the several simulations, demanded great effort in order for behaviour to be understood, since at first glance they were not as easily correlated between each other as expected. Due to that, a more extensive knowledge had to be done regarding the double sideband systems, on the pursuit of fully understanding everything about the performance of the system.

Had it been possible to study the system even at more detail it might have been possible to trace the behaviour of the results and even project the consequences of the variation of certain parameters.It seems that there exists 3 main parameters that hugely affect the performance of the RoF signal on the optical field and those are, as it has been mentioned previously, the carrier frequency, the baud rate and the fiber length and therefore had it been possible it would be of interest to obtain a 3D plot with the results based on the variation of these parameters.

Chapter 4

Pratical Experiment

On this section the several experiments that were made on the laboratory are going to be described and analysed. The starting point consisted on performing both experiments witBOSA and RoF.

4.1   BOSA experiments

Back on the section 2.2, the fundamentals of the BOSA transceivers and their importance were briefly discussed. The measures that are going to be detailed next were performed before the implementation of the RF signal had even started. The purpose consisted on initiating the experimentation with the BOSA, but with a less complexed signal, Non-return-to-zero, NRZ, to get a more in-depth knowledge of the real results that can be obtained with the BOSA.

Due to the limitations of the material availabe at this stage it was only possible to study the behaviour of the transmitter, TOSA. The setup which can be observed below,4.1 was designed in order to proceed for the simulation of the upstream direction. Since, there was only a single TOSA at disposable, it was only possible to study an only-channel case, instead of 4 channels situation, which is the case for NG-PON2.
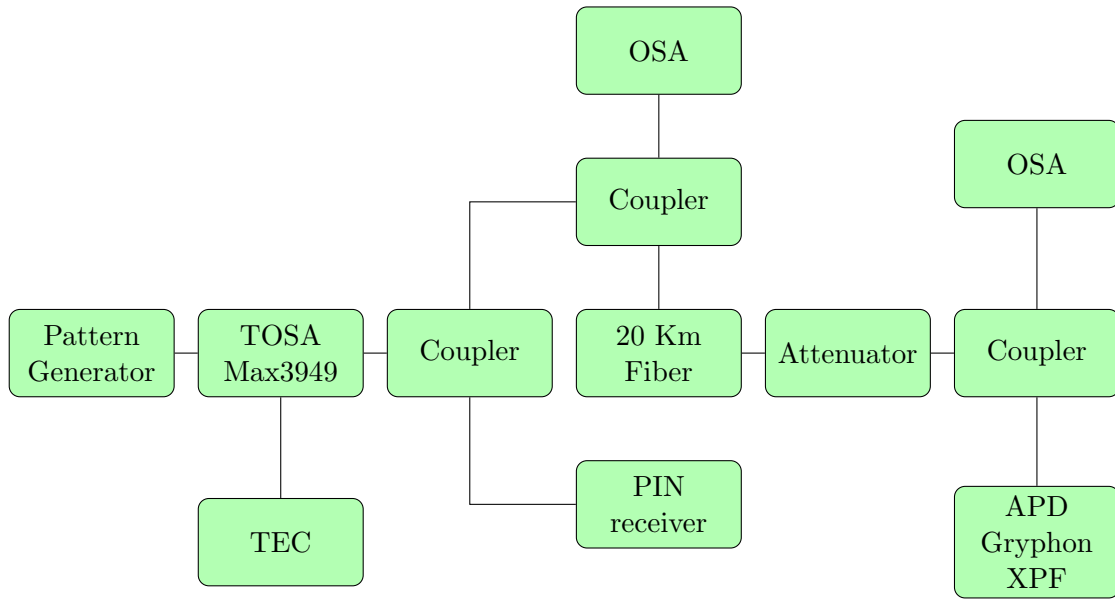
Figure 4.1: TOSA Upstream Experiment

Regarding the performance of the TOSA, there are 3 important parameters and those are both the BIAS and MOD current but also the temperature. The current that is set on the laser is controlled by a software, where it's possible to change both parameters and therefore affect the performance of the TOSA.
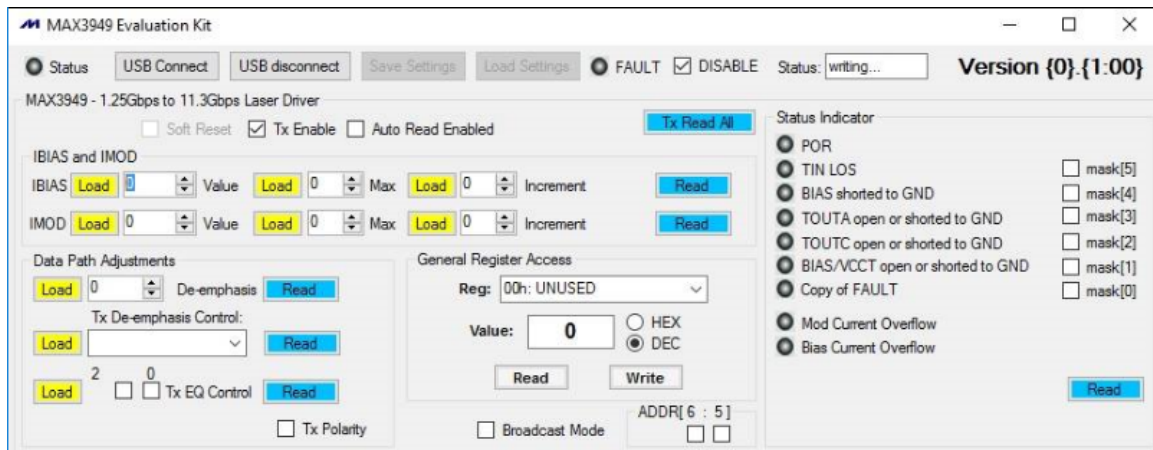

Figure 4.2: Software used to control the current of the BOSA

As already mentioned the TOSA performance changes with the temperature, more concretely the wavelength that is propagated. The device responsible for setting the temperature on the TOSA to the desired point is denominated of TEC.

In figure 4.3, it's possible to manly observe the impact that the temperature has on the wavelength that is propagated and that for the same set of pair value for I_{BIAS} and I_{MOD} it's possible to observe that the increase of the temperature will also increase the correspondent wavelength that the laser is going to emit at.
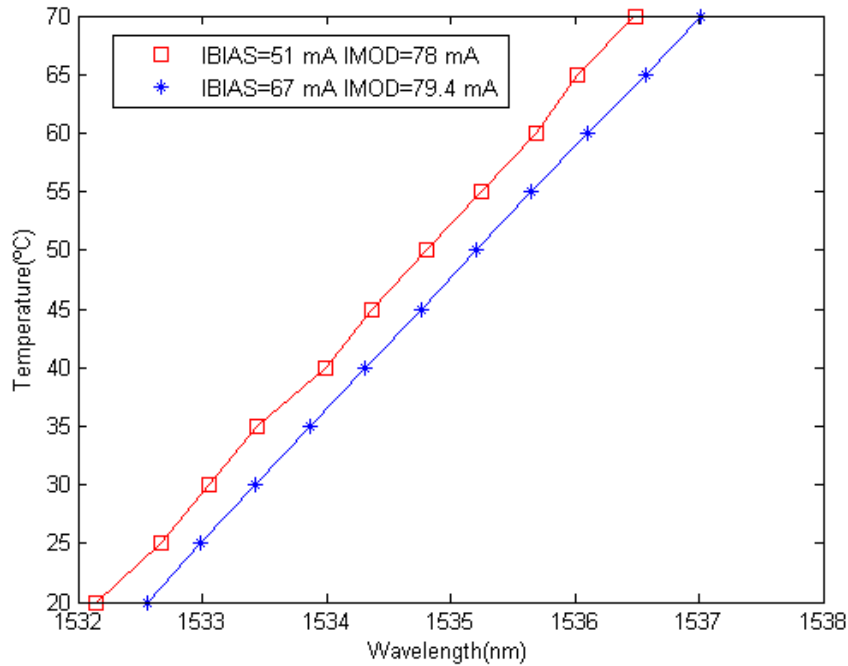
Figure 4.3: TEC characterization for a pair of currents

As it was already mentioned the objective of these simulations were to analyse the performance of the TOSA for the 4 upstream wavelengths defined by the NG-PON2 standardization, which are:

Table 4.1: Upstream Wavelength Channels

λ_1	1532.690	nm
λ_2	1533,473	nm
λ_3	1534,255	nm
λ_4	1535,037	nm

The pattern generator as the name suggests is the device responsible for generating the signal which is going to be directly modulated by the TOSA, which basically consisted on a NRZ signal with 10 Gbits/s. The pattern generator was also responsible for showing the estimation of BER that the system presented, and the following graphics were obtained by changing the optical power received and noting the respective BER value obtained.

The only considerations that were taken was that the signal generated should present an extinction ratio of around 6 dB. ER consists on the ratio of the energy that is used to transmit the logic level '1' in comparison to the logic level '0', as it can be seen by the following expression:

$$ER = 10log_{10}\frac{'1'powerlevel}{'0'powerlevel} \tag{4.1}$$

The ER has impact on the performance of the system, since an higher ER for the same average power signal will lead to better results, because the power for level '1' and level '0'
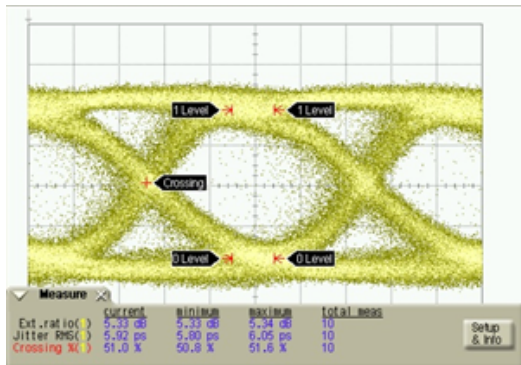
are more distanced, which means an higher modulation power, and consequently it becomes easier for the signal to be successfully recovered by the receiver. Instead of the ROSA as receiver, an APD board was used.
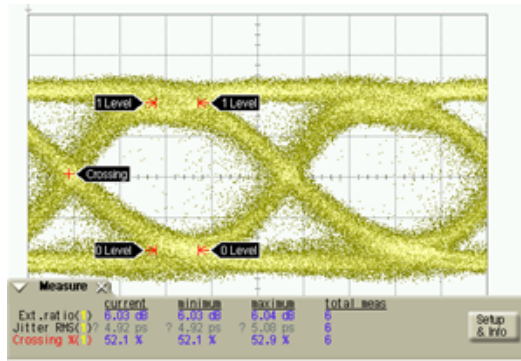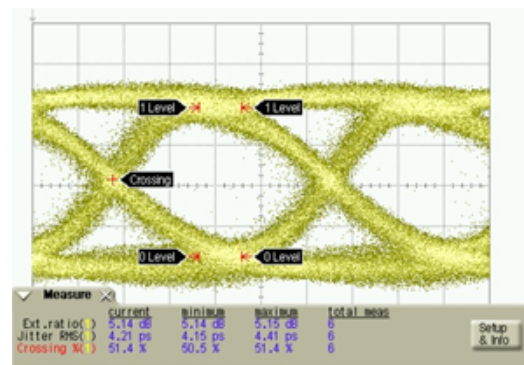

(a) Eye Diagram obtained for the propagation of λ_1
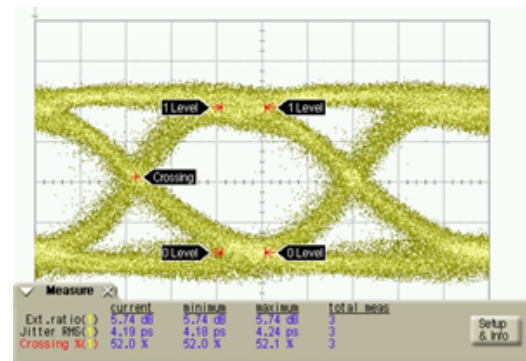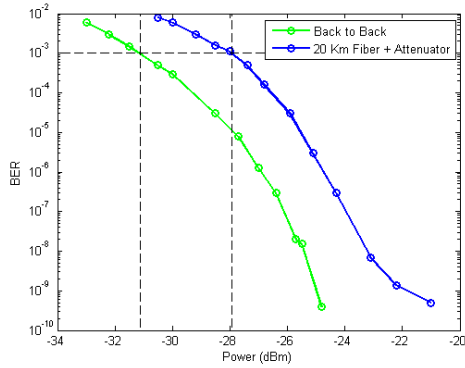

(b) Eye Diagram obtained for the propagation of λ_2

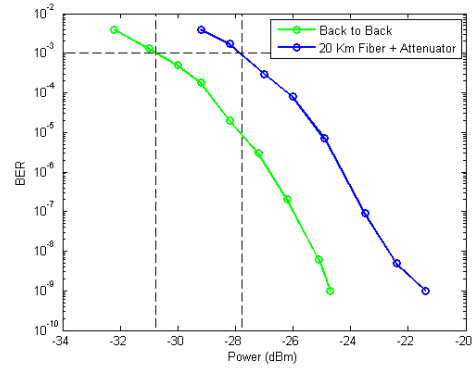(c) Eye Diagram obtained for the propagation of λ_3

(d) Eye Diagram obtained for the propagation of λ_4

Figure 4.4: Eye Diagram obtained for the several λ propagated

By observing 4.4, it's possible to conclude that the ER obtained with the increase of the temperature and consequently of the wavelength propagated because farther away for the 6 dB meta. Truthfully told, it was possible to obtain the 6 dB, for some pair values of I_{MOD} and I_{BIAS}, but the general aspect of the eye diagram was not satisfactory. One of the reasons for that, is the fact that the TOSA studied consists on a DML and it's highly affected by chirp, both adiabatic and transient, which obviously affects the performance of the system.
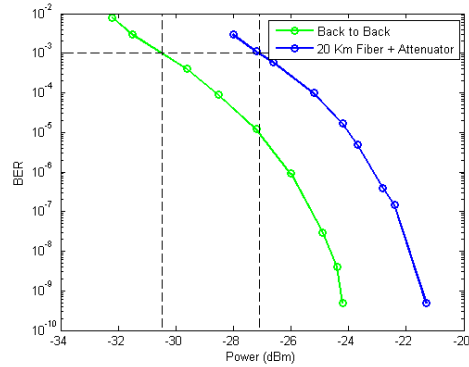
(a) BER vs Power obtained for the propagation of λ_1

(b) BER vs Power obtained for the propagation of λ_2
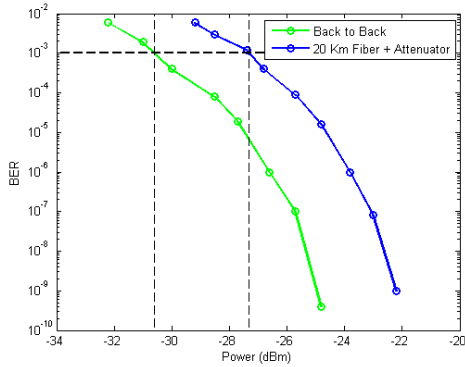
(c) BER vs Power obtained for the propagation of λ_3

(d) BER vs Power obtained for the propagation of λ_4

Figure 4.5: BER vs Power obtained for the several *lambda* propagated

By analysing the graphics we conclude that the behaviour it's practically the same for the different wavelengths, though with the decrease of the ER, the instant of minimum power where the BER reaches the limit onto which the signal will not be able to be recovered to the original conditions, slightly shifts to an higher power, which means the system has lost sensibility.

Another conclusion is that, if we compare the results obtained for the B2B and 20 Km, it's possible to conclude that there exists a power penalty of approximately 1.5 dB, because that is the the quantity of power that the receiver needs more for the 20 Km situation in comparison with the absence of fiber for the same BER results to be attained. This power penalty is explained because of the negative impact that the chirp has on the dispersion, which causes the system to behave a lot worse compared to a situation where unchirped pulses are employed [49].

4.2 RoF experiments

The main objective from the practical experiment consisted on mounting a setup similar to the one modelled on the simulation platform. On figure 4.6 it's possible to observe the setup used for the experiments and the respective block diagram in 4.7,
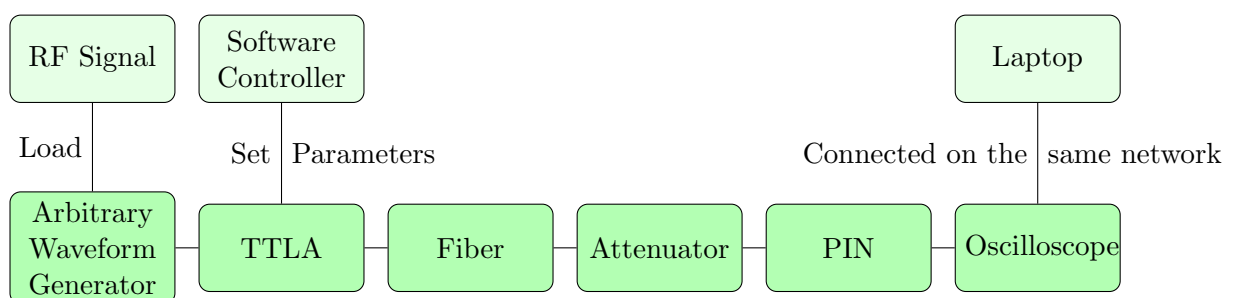

Figure 4.6: Laboratory RoF experiment

Figure 4.7: TOSA Upstream Experiment

The first process consisted on loading the signal onto the AWG. The AWG is then connected to the TTA, which consists on LASER plus mach-zehnder modulator system. The TTA is connected to a laptop by an USB cable, and using a program it's possible to configure its parameters, with the BIAS current being the most important, since it will have major impact on the performance of the TTA. With the TTA turned on, the signal is finally propagated onto the optical system, where it will go through the fiber with the specific length

desired. If the system studied its B2B there will be no fiber connected on the optical system. After the fiber, an attenuator is added to change the optical power which is then received on the photodiode. For last, the output of the PIN is connected to one of the channels of the oscilloscope, so it's possible to observe in real time how the signal was received on the PIN. For the purpose of the practical work, the approach chosen was to capture as many as windows as possible from the Oscilloscope. To achieve that, a laptop had to be configured to be on the same network as the oscilloscope, and using a matlab script it was possible to connect to the oscilloscope and remove the number of windows desired. There exists some restrictions to the number of samples that can be sent to the AWG, therefore the characteristics of each modulation format signal were not the same for each signal.

The objective consisted to create signals with close to 10^4 bits and to take 100 windows continuously from the oscilloscope, so the system would be studied for approximately 10^6 bits. The 100 windows of retrieved signals from the oscilloscope were saved on a three-dimensional vector, which consequently was saved as a mat file.

In order to analyse the signals, the process consisted on first loading the file for respective generated signal and then load the file which contains the 100 windows of the received signal for a certain optical power at the receiver.

In figure 4.8, one window of the received signal is being processed and analysed by the evaluations metrics that have been already mentioned.
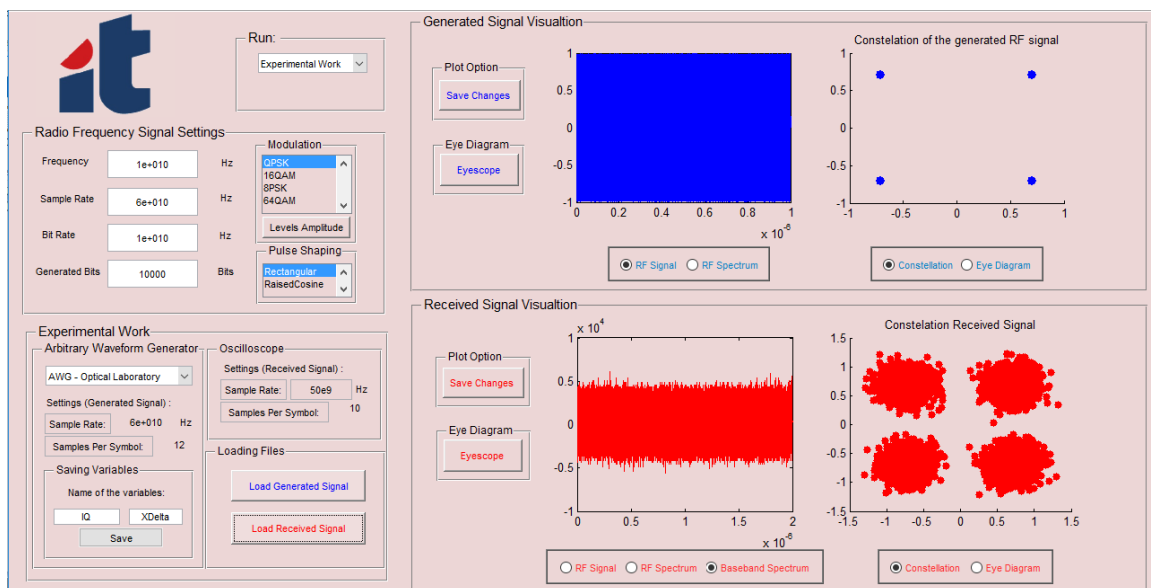

Figure 4.8: Simulation Platform running a loaded file

The evaluations metrics are going to be performed for the number of windows taken, and while the EVM is obtained by the mean of the value calculated for each window, the process for the bit error consists on keep creasing the quantity of errors and then do the calculation by dividing the number of errors by the number of bits analysed.

The signal generated for the QPSK modulation format was loaded onto the AWG and is represented in the figures 4.9 and its parameters in 4.2

Table 4.2: QPSK modulation format parameters signal

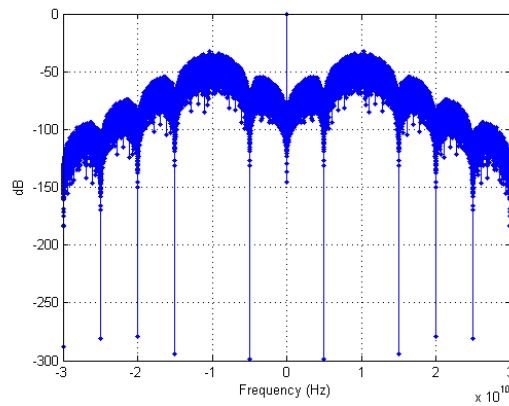| Frequency Carrier	10	GHz
Number of Bits	10e4	bits
Data Rate	10	Gbits/s

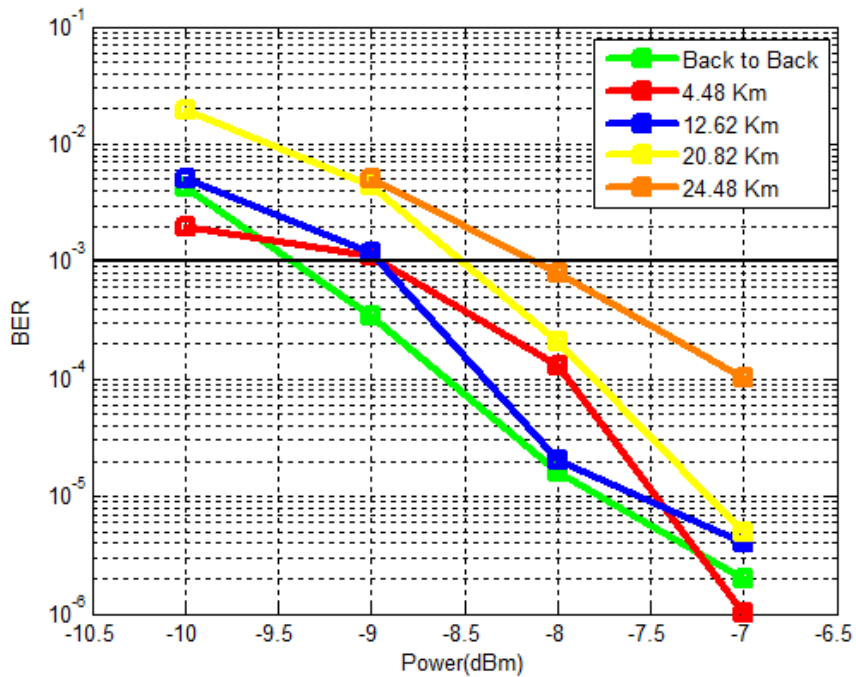Figure 4.9: QPSK modulation format RF signal loaded onto the AWG

Figure 4.10: Laboratory QPSK RoF experiment, Power vs BER

The RF signal with 16-QAM modulation format was loaded on the AWG with the following parameters of table 4.3

Table 4.3: 16-QAM modulation format parameter signal

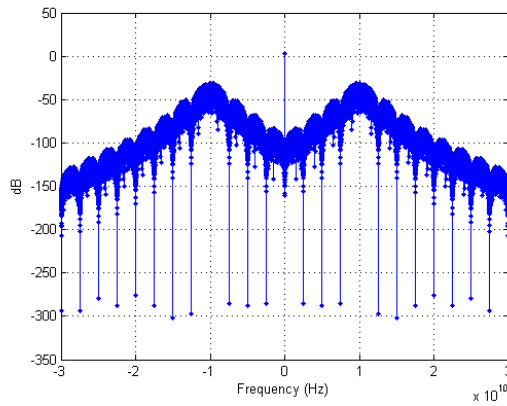| Frequency Carrier	10	GHz
Number of Bits	10e4	bits
Data Rate	10	Gbits/s

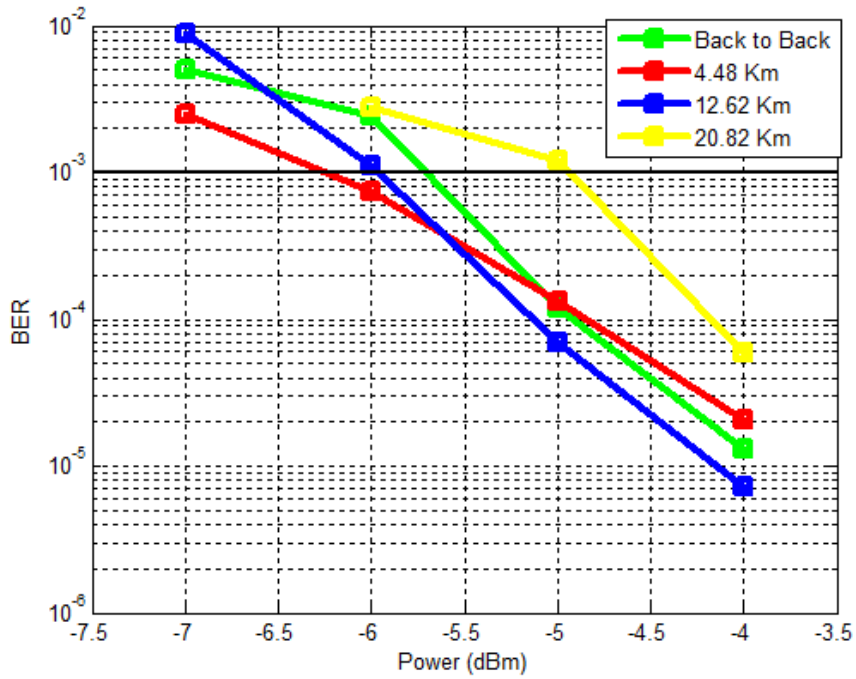Figure 4.11: Spectrum of the 16-QAM modulation format RF signal loaded onto the AWG

Figure 4.12: Laboratory 16-QAM RoF experiment, Power vs BER

Table 4.4: 8-PSK modulation format parameter signal

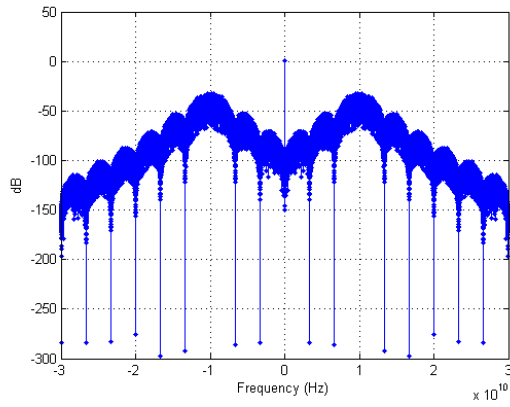| Frequency Carrier	10	GHz
Number of Bits	9.6e4	bits
Data Rate	10	Gbits/s

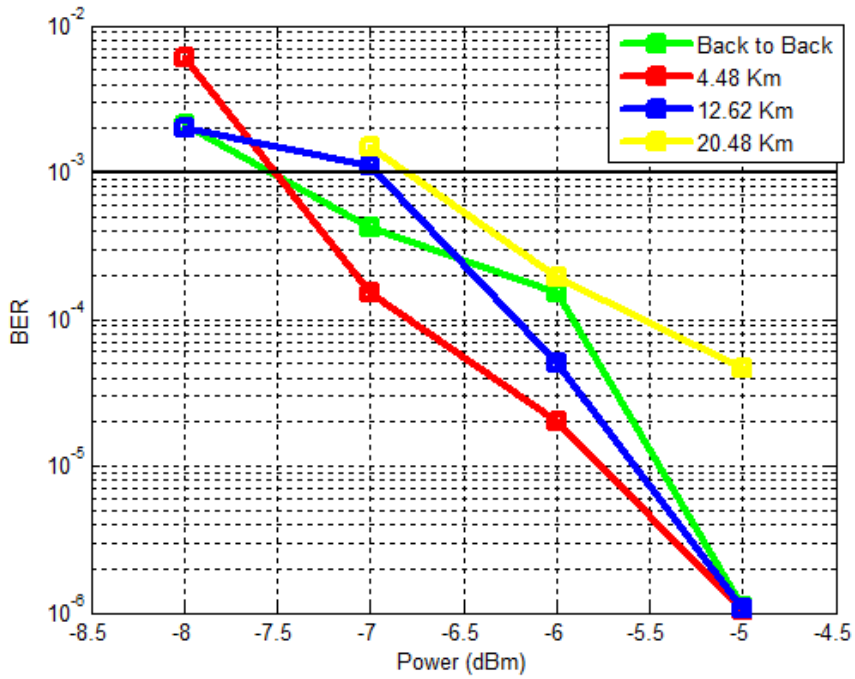Figure 4.13: Spectrum of the 8-PSK modulation format RF signal loaded onto the AWG

Figure 4.14: Laboratory 8-PSK RoF experiment, Power vs BER

Table 4.5: 64-QAM modulation format parameter signal

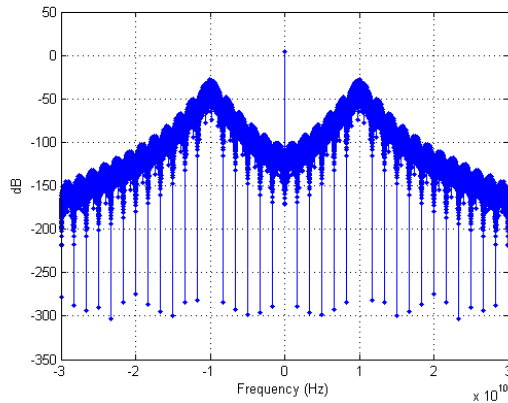| Frequency Carrier	10	GHz
Number of Bits	10e4	bits
Data Rate	10	Gbits/s

Figure 4.15: Spectrum of the 64-QAM modulation format RF signal loaded onto the AWG

Regarding the 64-QAM, it's possible to visualize the spectrum of the generated signal, but since the reception for it still had some problems, which were not solved, this modulation format was discarded.

The primary objective of the tests done above consisted on analysing the impact of fiber for the different modulation formats. But there are limitations when performing this simulations at the laboratory.Having to add a fiber block, increase the already existing one with another block, adding/removing connectors or even impurities that start to arise on the fiber (constantly needed to clean it), are all factors that change the optical power that is being received at the photodiode. The objective consisted to analyse all the setups with the exactly same optical power, but it was practically impossible when the setup has to be constantly changed.

Due to the reason mentioned above and the fact that the system by itself isn't that sensible, this highly affects the precision of the results that can be taken, which is the reasons for the variation that it's possible to be seen for the situation of B2B, 4.48 km and 12.62 km of fiber, for the three modulation formats studied. Therefore, the conclusion obtained is that even for the fiber block length of 12.62 km, chromatic dispersion effect hasn't visibly affected the results of the system. On other hand, the same can't be said for the 20.48 km, where it's possible to observe that the performance of the system is worse, and a power penalty certainly exists compared to the lower fiber lengths tested.

On the following graphics it's possible to observe another perspective of the results. Instead of analysing the same format modulation for the several fiber lengths, on this graphics we visualize the performance of the modulation formats tested for the same fiber length and for a varying optical power received. These results are more precise, due to the fact that for
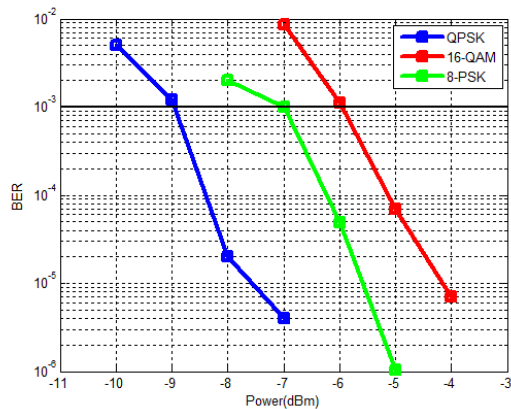
a measure of an optical power received, the only thing needed to change on the system was the signal loaded to the AWG, which gives a guarantee that the different signals are being analysed for the exact same conditions.
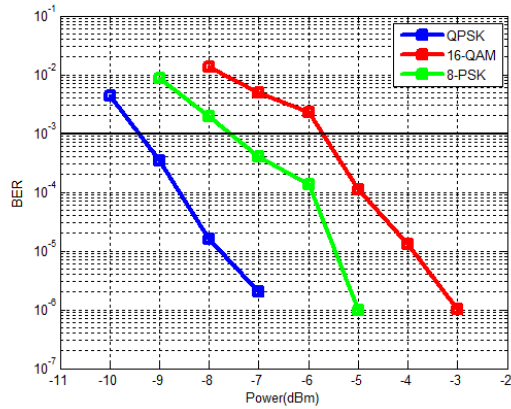
(a) B2B
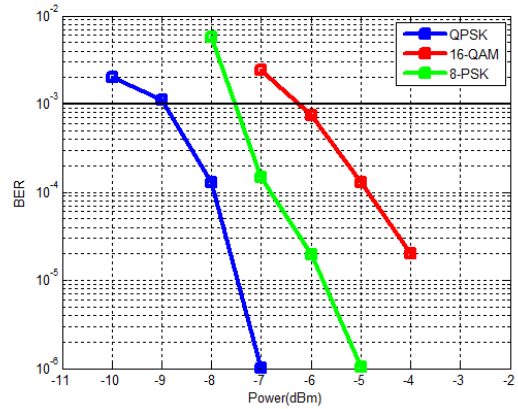
(b) 4.48 Km of fiber

(c) 12.62 Km of fiber
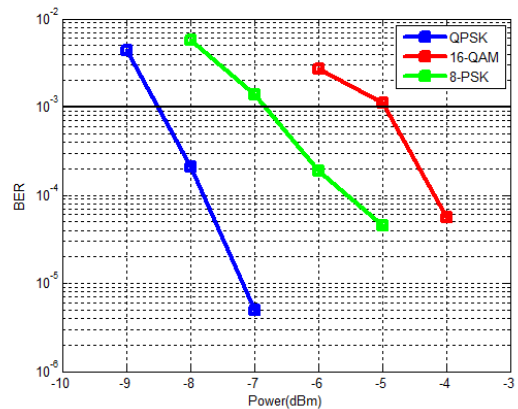
(d) 20.82 Km of fiber

Figure 4.16: Laboratory RoF experiment, Power vs BER, comparison of the different modulation formats for different fiber lengths

It's possible to observe that the with the increase of the complexity of the signal, the sensitivity of the system consequently lowers, and the explanation for such occurrence consists on the fact that with the increase of the complexity of the modulation format, the signal becomes less tolerant to noise. For that reason, the results obtained for QPSK modulation format show the better results, followed by 8-PSK and by last the 16-QAM. If 64-QAM had been completely implemented, the results obtained for it, would be the worst of all, for the reason that has been mentioned.

4.3 Bandwidth of the System

The results obtained on the laboratory are highly dependent on the conditions that define the RF signal that is being generated. At this section, concretely, the purpose consists on analysing the consequences of the spectrum of the signal which is desired to transmit. Both the AWG and the Mach-Zehnder obviously don't have unlimited bandwidth. The latter has a bandwidth of 10GHz, which means that at 10GHz, the cut-off frequency, a 3dB loss is imposed on the signal by the low-pass filter.

The purpose of the next graphic consists on displaying a comparison between the sensibility of the setup with an RF carrier of 6 GHz and 10 GHz.

Table 4.6: 16-QAM modulation format parameter signal

Frequency Carrier	6	GHz	Frequency Carrier	10	GHz
Number of Bits	10e4	bits	Number of Bits	10e4	bits
Data Rate	10	Gbits/s	Data Rate	10	Gbits/s
Baud Rate	2.5	Gbits/s	Baud Rate	2.5	Gbits/s
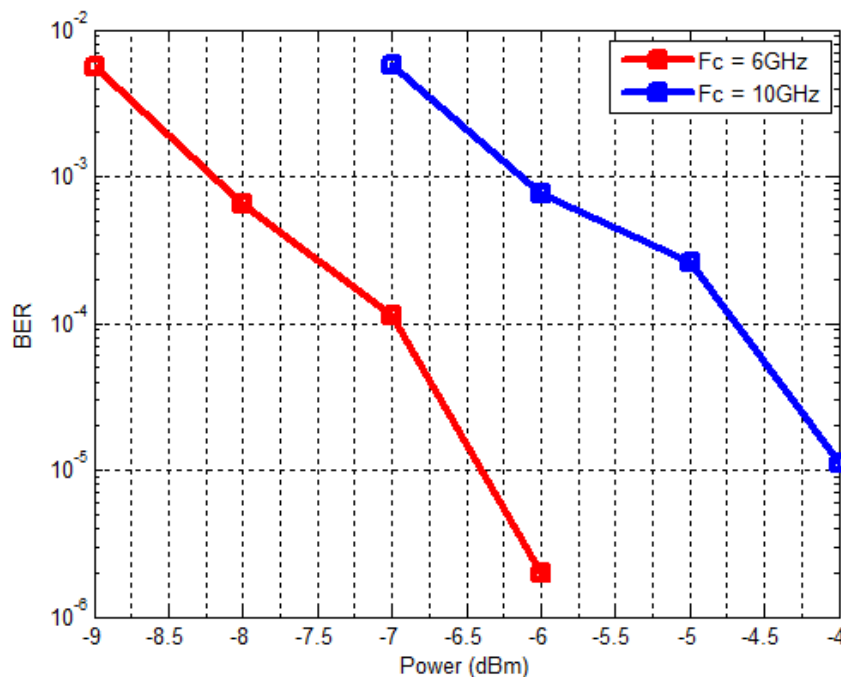
Figure 4.17: Comparison between the performance of the system on
B2B for two different frequency carriers

As expected, the system is a lot more sensitive to the lower frequency 6 GHz than for 10 GHz and the reason is the one that has been mentioned above. The low-pass filter attenuated significantly more the signal for frequency carrier of 10 GHz, therefore the noise added by the PIN degrades the signal more, consequently lowering the sensibility of the system. The power penalty observed between these 2 carrier is approximately quantified in 2dB. So it can

be concluded that the frequency carrier of 10GHz, with the setup which was mounted, is not the most adequate frequency carrier to have the better results, but since the response of an real low-pass filter isn't abrupt at the cut-off frequency, it was still possible to obtain results and take conclusions from it.

Chapter 5

Conclusion and Future Work

The first conclusion which was taken on the development of this dissertation consisted on the fact that NG-PON2 is undoubtedly the future for optical access network.

The new emerging wireless systems, which will be integrated with optical fiber are much likely, capable of being supported by the Radio-over-Fiber technology, as it was mentioned when the topic of 5G was touched on, since it has the potential of ensuring an optimized radio coverage, by enabling the efficient delivery of the high bit data rate wireless signals to a large number of wireless access points.

On this context, this dissertation had the objective of performing experiments on this subject by resorting to simple setups, which were analysed on both simulation, with the successful implementation of a graphic environment simulator, but as well on the laboratory.

Regarding the performance of the system that was made on this document, there still needs to be done a deeper characterization of the performance of the system, so it can be possible to project the expected performance of the RoF signal based on the characteristics, of not only the signal, but also the optical system.

It was concluded that the double sideband signal is heavily affected with chromatic dispersion, but this affect is more noticeable at certain carrier frequencies and data rate.

At the beginning the system was studied more the characteristis onto which it is defined for the NG-PON2 standard, but due to the fact that it is easier affect by dispersion at those lowers frequencies and baud rates the system was studied for other different parameters values.

Regarding the modulation formats it was concluded that QPSK is the one who gives the best performance, due to the fact that it has an higher tolerance to impact on the quality of the signal, followed by 8-PSK and in last 16-QAM.

As future work, i would make the following suggestions:

- Continuation of the work developed on the platform by turning it more robust but also implement new models and perform more complex simulations.

- Create a new board for the BOSA, so it's possible to analyse it with an analog signal instead of only with a digital one.

- Perform experiments with a more complex system that allows for a more profound characterization of the system.

- Analyse the best method to transform the DSB signal onto a SSB one, and obtain the following advantages and disadvantages of each situation.

Bibliography

[1] Nathan J Gomes, Paulo P Monteiro, and Atílio Gameiro. *Next generation wireless communications using radio over fiber*. John Wiley & Sons, 2012.

[2] Derek Nesset. Ng-pon2 technology and standards. *Journal of Lightwave Technology*, 33 (5):1136–1143, 2015.

[3] Leonid G Kazovsky, Ning Cheng, Wei-Tao Shaw, David Gutierrez, and Shing-Wa Wong. *Broadband optical access networks*. John Wiley & Sons, 2011.

[4] Fiber transceiver solution. `http://www.fiber-optic-transceiver-module.com/brief-introduction-to-tosa-rosa-and-bosa.html`. Accessed: 2016-07-15.

[5] Hamed Al-Raweshidy and Shozo Komaki. *Radio over fiber technologies for mobile communications networks*. Artech House, 2002.

[6] Radio-over-fibre techniques and performance. `http://cdn.intechopen.com/pdfs-wm/8432.pdf`. Accessed: 2016-04-10.

[7] Anthony Ng'oma. *Radio-over-fibre technology for broadband wireless communication systems*. Technische Universiteit Eindhoven, 2005.

[8] Gerd Keiser. *Optical fiber communications*. Wiley Online Library, 2003.

[9] R Karthikeyan and S Prakasam. A survey on radio over fiber (rof) for wireless broadband access technologies. *International Journal of Computer Applications*, 64(12), 2013.

[10] D Opatić. Radio over fiber technology for wireless access.

[11] Schematic highlighting three possible schemes for radio signal transport between the central office and remote access point in hfr systems. `http://www.nature.com/nphoton/journal/v1/n6/fig_tab/nphoton.2007.89_F3.html`. Accessed: 2016-02-15.

[12] Ampalavanapillai Nirmalathas, Prasanna A Gamage, Christina Lim, Dalma Novak, and Rodney Waterhouse. Digitized radio-over-fiber technologies for converged optical wireless access network. *Journal of Lightwave Technology*, 28(16):2366–2375, 2010.

[13] Ahmed I Zayed. *Advances in Shannon's sampling theory*. CRC press, 1993.

[14] Luis M Pessoa, Joana S Tavares, Diogo Coelho, and Henrique M Salgado. Experimental evaluation of a digitized fiber-wireless system employing sigma delta modulation. *Optics express*, 22(14):17508–17523, 2014.

[15] Xianbin Yu, Timothy B Gibbon, and Idelfonso Tafur Monroy. Compact wireless access nodes for wdm bidirectional radio-over-fiber system based on rsoa. In *Optical Fiber Communication Conference*, page OWP1. Optical Society of America, 2009.

[16] David Wake, Anthony Nkansah, Nathan J Gomes, Guilhem De Valicourt, Romain Brenot, Manuel Violas, Zhansheng Liu, Filipe Ferreira, and Silvia Pato. A comparison of radio over fiber link types for the support of wideband radio channels. *Lightwave Technology, Journal of*, 28(16):2416–2422, 2010.

[17] A Powell. Radio over fiber technology: Current applications and future potential in mobile networks–advantages and challenges for a powerful technology. *Radio over Fiber Technologies for Mobile Communications Networks, H. Al-Raweshidy, and S. Komaki, ed.(Artech House, Inc, USA, 2002)*, 2002.

[18] Jyoti C Shrestha, Sven Blom, Bernd Witzigmann, and Hartmut H Hillmer. Investigation of relative intensity noise in asymmetric external cavity semiconductor laser sensors: Influence of dual-line spectral separation and linewidth enhancement factor. *Sensors Journal, IEEE*, 15(11):6619–6624, 2015.

[19] Toshiaki Suhara. *Semiconductor laser fundamentals*. CRC Press, 2004.

[20] Ali Kabalan, Salim Faci, Anne-Laure Billabert, Frédérique Deshours, and Catherine Algani. Direct and external modulation of if over fiber systems for 60 ghz wireless applications. *International Journal of Microwave and Wireless Technologies*, pages 1–6, 2015.

[21] Understanding intermodulation distortion measurements. `http://electronicdesign.com/communications/understanding-intermodulation-distortion-measurements`. Accessed: 2016-07-17.

[22] Yan Cui, Yitang Dai, Feifei Yin, Jian Dai, Kun Xu, Jianqiang Li, and Jintong Lin. Intermodulation distortion suppression for intensity-modulated analog fiber-optic link incorporating optical carrier band processing. *Optics express*, 21(20):23433–23440, 2013.

[23] Optical fiber dispersion. `https://www.fiberoptics4sale.com/blogs/archive-posts/95047942-optical-fiber-dispersion`, . Accessed: 2016-07-17.

[24] Preetpaul S Devgan, Dean P Brown, and Robert L Nelson. Rf performance of single sideband modulation versus dual sideband modulation in a photonic link. *Journal of Lightwave Technology*, 33(9):1888–1895, 2015.

[25] Graham H Smith, Dalma Novak, and Zaheer Ahmed. Overcoming chromatic-dispersion effects in fiber-wireless systems incorporating external modulators. *IEEE transactions on microwave theory and techniques*, 45(8):1410–1415, 1997.

[26] Optical fiber attenuation. `https://www.fiberoptics4sale.com/blogs/archive-posts/95052294-optical-fiber-attenuation`, . Accessed: 2016-06-18.

[27] Abdelhakim Boudkhil and Belabbes Soudini. Analysis of fundamental photodetection noises and evaluation of pin and apd photodiodes performances using an optical high debit transmission chain simulated by optisystem. *International Journal of Computer Applications*, 115(18), 2015.

[28] Daisuke Iida, Shigeru Kuwano, Jun-ichi Kani, and Jun Terada. Dynamic twdm-pon for mobile radio access networks. *Optics express*, 21(22):26209–26218, 2013.

[29] Rosinei S Oliveira, Diogo FR Viana, Mario Lima, Carlos RL Francês, Antonio Teixeira, and João CW A Costa. Digital radio over fiber system in the ng-pon2 context. *Journal of Microwaves, Optoelectronics and Electromagnetic Applications (JMOe)*, 14:179–193, 2015.

[30] CPRI Specification. V4. 2. *Common Public Radio Interface (CPRI)*, 2010.

[31] Understanding the basics of cpri fronthaul technology. `www.cnrood.com/amfilerating/file/download/file_id/1625`. Accessed: 2016-02-20.

[32] Haoshuo Chen, Jiajun Ye, and Rujian Lin. *Millimeter-wave Radio over Fiber System for Broadband Wireless Communication*. INTECH Open Access Publisher, 2010.

[33] Maged Elkashlan, Trung Q Duong, and Hsiao-Hwa Chen. Millimeter-wave communications for 5g: fundamentals: Part i [guest editorial]. *Communications Magazine, IEEE*, 52(9):52–54, 2014.

[34] Yong Niu, Yong Li, Depeng Jin, Li Su, and Athanasios V Vasilakos. A survey of millimeter wave communications (mmwave) for 5g: opportunities and challenges. *Wireless Networks*, 21(8):2657–2676, 2015.

[35] Felix Gutierrez Jr, Shatam Agarwal, Kristen Parrish, and Theodore S Rappaport. On-chip integrated antenna structures in cmos for 60 ghz wpan systems. *Selected Areas in Communications, IEEE Journal on*, 27(8):1367–1378, 2009.

[36] Bin Wang, Li Chen, Xiaohang Chen, Xin Zhang, and Dacheng Yang. Resource allocation optimization for device-to-device communication underlaying cellular networks. In *Vehicular Technology Conference (VTC Spring), 2011 IEEE 73rd*, pages 1–6. IEEE, 2011.

[37] Rakesh Taori and Arun Sridharan. Point-to-multipoint in-band mmwave backhaul for 5g networks. *Communications Magazine, IEEE*, 53(1):195–201, 2015.

[38] Square-root raised cosine signals (srrc). `http://www.navipedia.net/index.php/Square-Root_Raised_Cosine_Signals_(SRRC)`. Accessed: 2016-02-20.

[39] Hoon Kim and Alan H Gnauck. Chirp characteristics of dual-drive. mach-zehnder modulator with a finite dc extinction ratio. *Photonics Technology Letters, IEEE*, 14(3):298–300, 2002.

[40] Govind P Agrawal. *Nonlinear fiber optics*. Academic press, 2007.

[41] Jing Shao, Xiaojun Liang, and Sudhakar Kumar. Comparison of split-step fourier schemes for simulating fiber optic communication systems. *Photonics Journal, IEEE*, 6(4):1–15, 2014.

[42] Wilmar Hernandez. Input-output transfer function analysis of a photometer circuit based on an operational amplifier. *Sensors*, 8(1):35–50, 2008.

[43] John G Proakis and Dimitris G Manolakis. *Digital Signal Processing: Principles, Algorithms, and Applications.* Prentice Hall, 1996.

[44] The nyquist sampling theorem. `http://www.spot.pcc.edu/~ghecht/Gary's%20Nyquist%20Document.pdf`. Accessed: 2016-02-20.

[45] HK Al-Musawi, WP Ng, Z Ghassemlooy, C Lu, and N Lalam. Experimental analysis of evm and ber for indoor radio-over-fibre networks using polymer optical fibre. In *Networks and Optical Communications-(NOC), 2015 20th European Conference on*, pages 1–6. IEEE, 2015.

[46] Understanding intermodulation distortion measurements. `http://electronicdesign.com/communications/understanding-intermodulation-distortion-measurements`. Accessed: 2016-05-5.

[47] Rene Schmogrow, Bernd Nebendahl, Marcus Winter, Arne Josten, David Hillerkuss, Swen Koenig, Joachim Meyer, Michael Dreschmann, Michael Huebner, Christian Koos, et al. Error vector magnitude as a performance measure for advanced modulation formats. *IEEE Photonics Technology Letters*, 24(1):61–63, 2012.

[48] Rishad Ahmed Shafik, Md Shahriar Rahman, and AHM Islam. On the extended relationships among evm, ber and snr as performance metrics. In *Electrical and Computer Engineering, 2006. ICECE'06. International Conference on*, pages 408–411. IEEE, 2006.

[49] Govind P Agrawal. *Lightwave technology: telecommunication systems.* John Wiley & Sons, 2005.

Appendix A

Matlab Simulation Platform

A.1 Matlab Simulation Outlook

Until now, on this chapter, it was first presented the steps followed for the generation and reception of a radio signal. The second step then consisted on modelling the several components that constitute an optical system, but in order to take the fullest potential out of the work that had been done for the simulation, it was decided to aggregate it with Matlab's Graphical User Interface (*GUI*), in order to have an interface where changing the characteristics of the radio signal, observing the results or even to perform different types of plottings would turn out to be as user friendlier as possible. The simulation plataform contains two main modes on which the program can be ran: simulation and experimental work. As the name suggest the *Simulation* option is chosen to simulate the propagation of a radio signal through the optical system and to analyse its state of reception. On figure 3.8, it's possible to visualize the outlook of the simulation mode implemented.
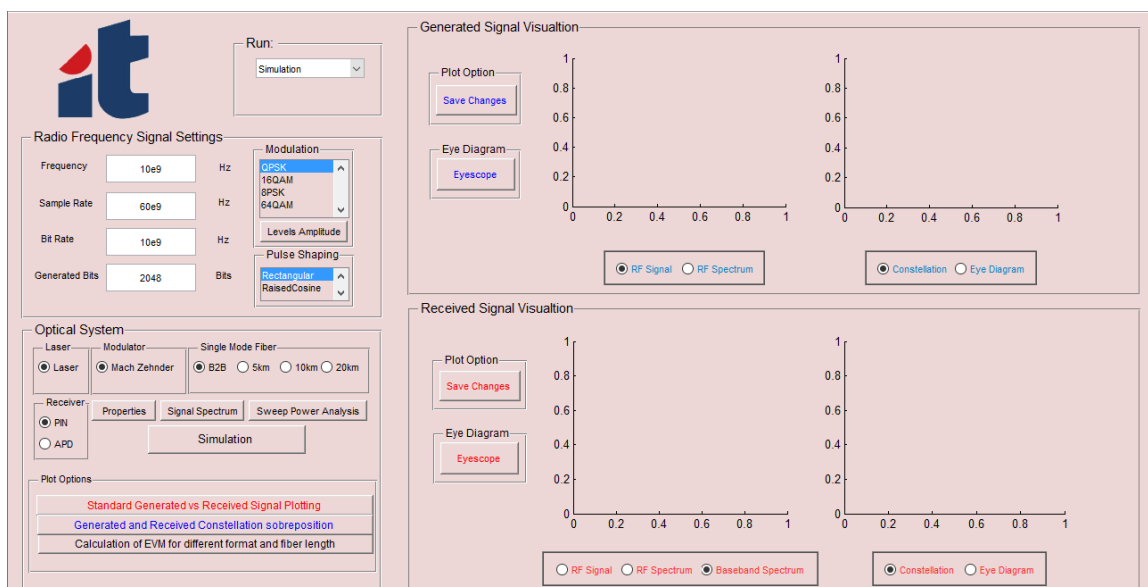

Figure A.1: Simulation Outlook

The radio frequency signal settings corresponds on the carrier frequency desired, the sam-

ple rate of the system, the defined bit rate and the generated number of bits.Since we are studying the NG-PON2 norm, the bit rate predefined corresponds to the 10 Gbits/s, and therefore this is one of the characteristics of the signal that for the simulations purpose isn't really of importance to change.Regarding the robustness of the results obtained, increasing the number of generated bits will also increase its feasibility, though it will raise the heaviness of the simulation. On the modulation panel is possible to change for the modulations formats implemented, and bellow on the pulse shaping it was planned to be possible to change between the rectangular pulse and raised cosine, but only the rectangular pulse shapping implementation is fully working.

Bellow, on the optical system panel, which is responsible of the modelling of the optical system, the only change that can be brought to the system, consists on the length of the optical fiber.

On the blocks for the visualization of the signals is possible to check the generated/received RF signal and their correspondent spectrum before/after being put on baseband. In the other figures is possible to observe either their constellations or the respective eye diagrams.

The *Experimental Work* is oriented to the processes that can help on the laboratory, such as the generation of the files which need to be loaded onto the AWG, retrieving the signal from the Oscilloscope and lastly to load a file which contains the generated signal and also load the received signal, which corresponds to the signal retrieved for the oscilloscope and study the performance of the system.
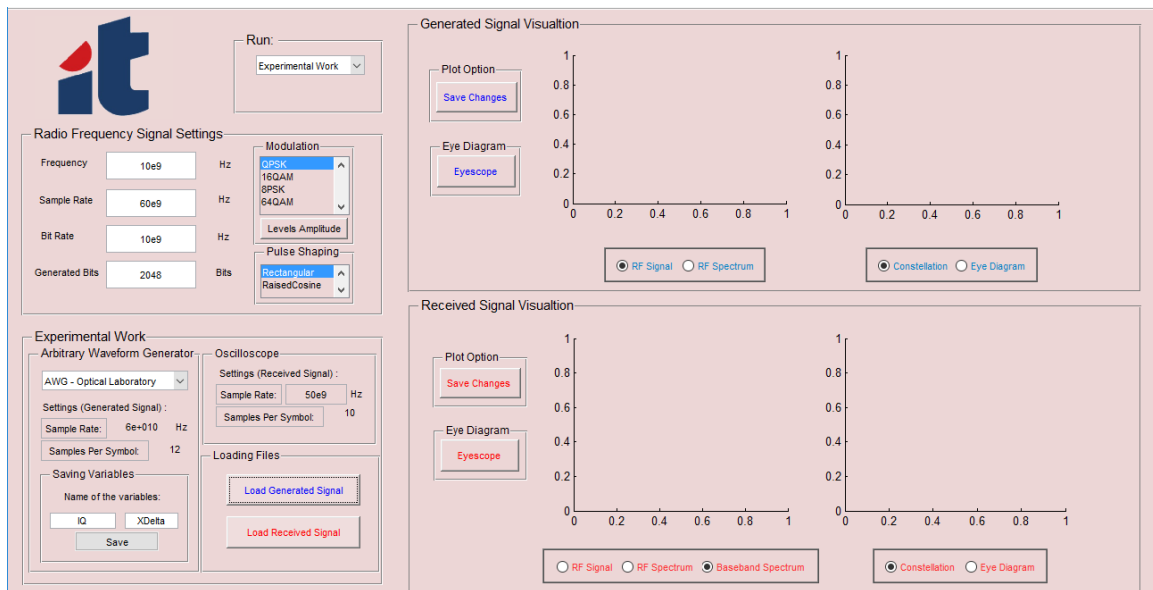

Figure A.2: Experimental Outlook

A.1.1 Properties

On this option is possible, not only to visualize the characteristics of each element of the optical system, but also to save if any alteration is made on the parameters of the optical system and perform new simulations with those new values.On the following figure is presented the interface, just as the values that were used to run the simulations,
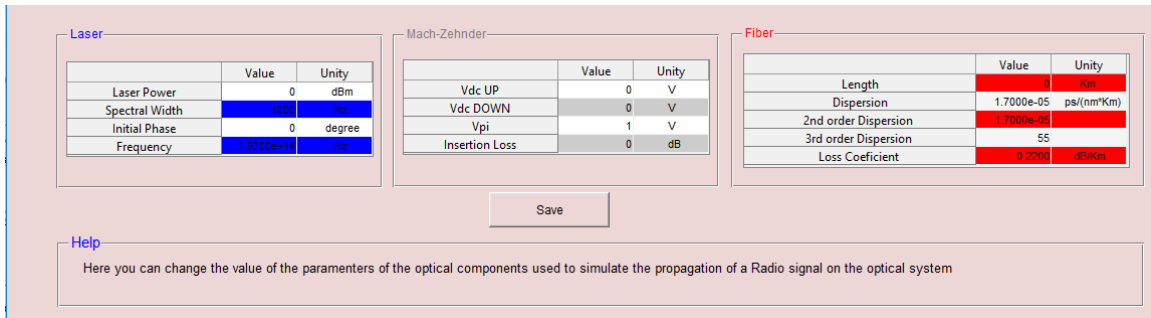

Figure A.3: Parameters properties

A.1.2 Signal Spectrum

After performing the simulation, by clicking on this pushbutton, it is shown the spectrum at the different stages of the optical system, but also the correspondent power signal, just like it would be possible to do with a power-meter on the laboratory.
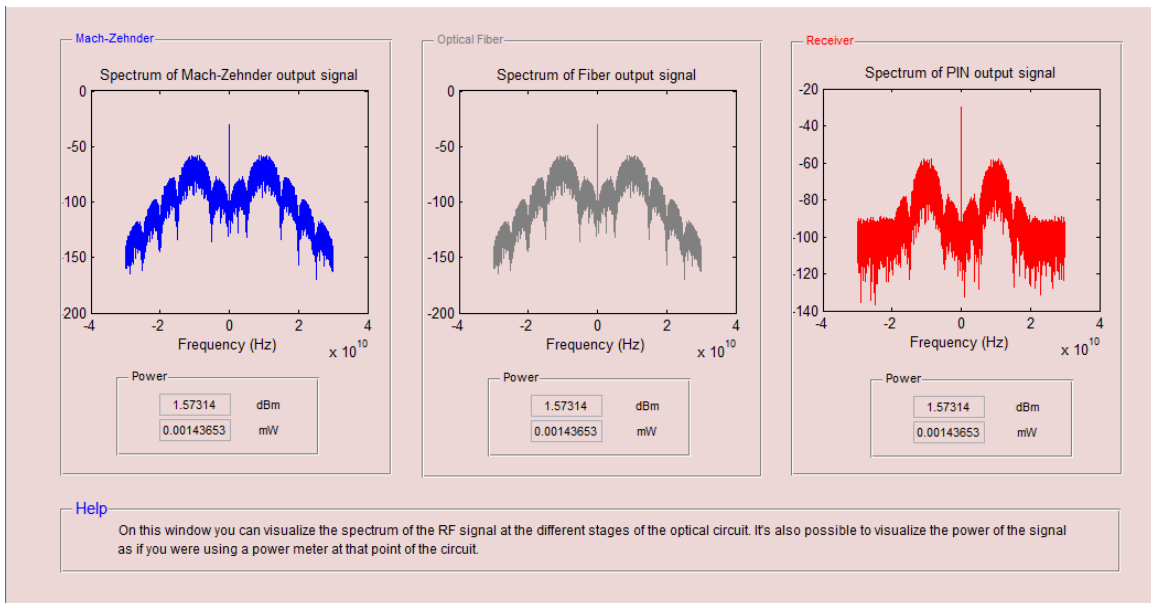

Figure A.4: Amplitude for the several modulations formats

On this case, since the simulation case had been B2B, no difference exists between the power at the output of the mach-zehnder and the output of the optical fiber model.

A.1.3   Levels Amplitude

As the name of this window indicates its possible to observe the amplitude levels for the different modulation formats. The location of the symbols is of major importance when referring to their respective constellations and at some situations it might be of interest to change their amplitudes for other values and if that is the case, it can be performed here on and then saved for the next simulations. In figure 3.11, it's possible to visualize the *gui* where you can perform this action,
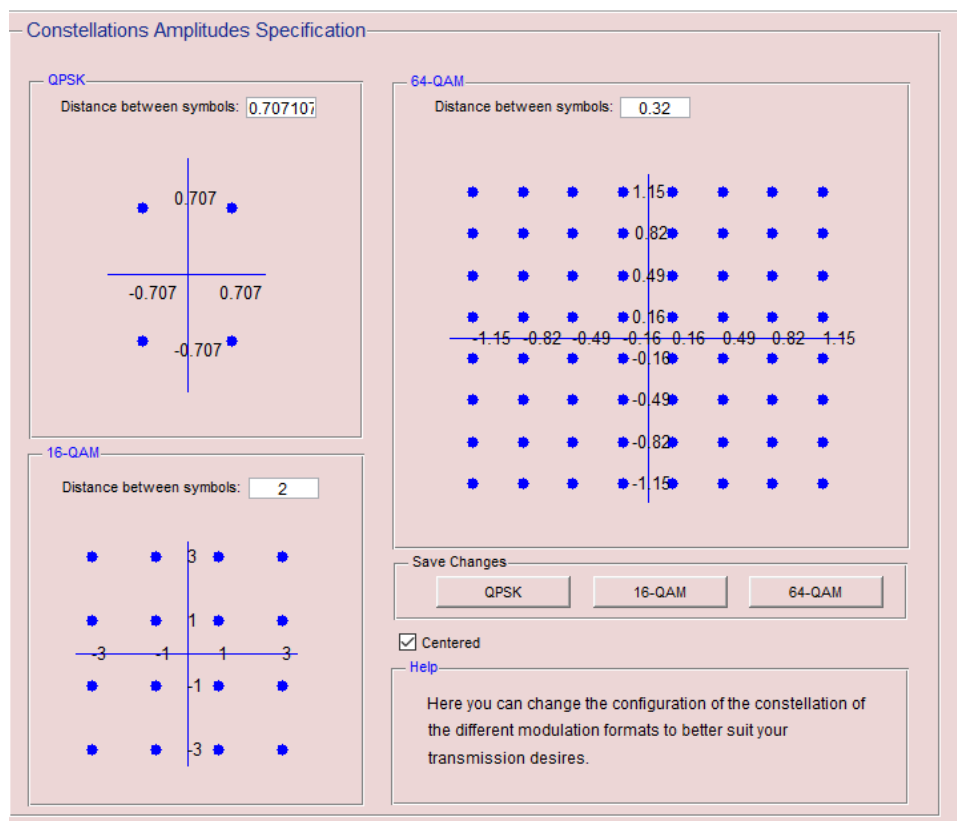

Figure A.5: Amplitude for the several modulations formats, except 8-PSK

A.1.4   Sweep Power Analysis

This window allows for the analysis of the system based on the optical power received, while the noise added to the signal on the photodiode keeps the same value. The consequences of lowering the power of the signal and maintaining the power of the noise added by the receptor, corresponds on a decrease of the signal to noise ratio, which means that the noise will affect more negatively the signal, and therefore the performance of the system will deteriorate. The objective from this power sweep attenuation is to be able to obtain the graphics that relates *BER* with the power at the receiver.
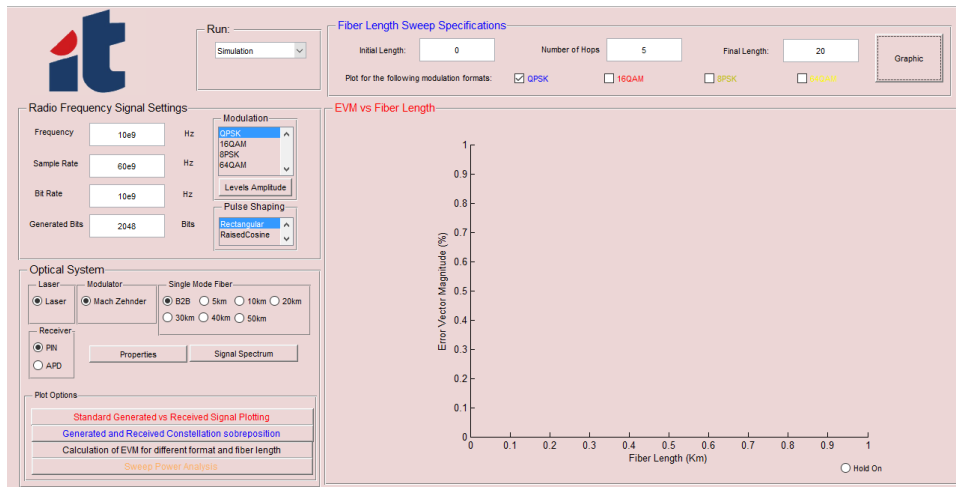
Figure A.6: Metrics results window

A.1.5 Sweep Fiber Length

On this section it's possible to obtain graphics that give a performance of the system with the fiber length, for the several modulation formats. The performance of the system is studied with the EVM metric and therefore it's possible to obtain a comparison between how the system performs with the increase of the fiber length. The only limitation, is that this was implemented, so the condition of the generated signal for all modulation formats selected are the same, which means, different Gbauds/s.
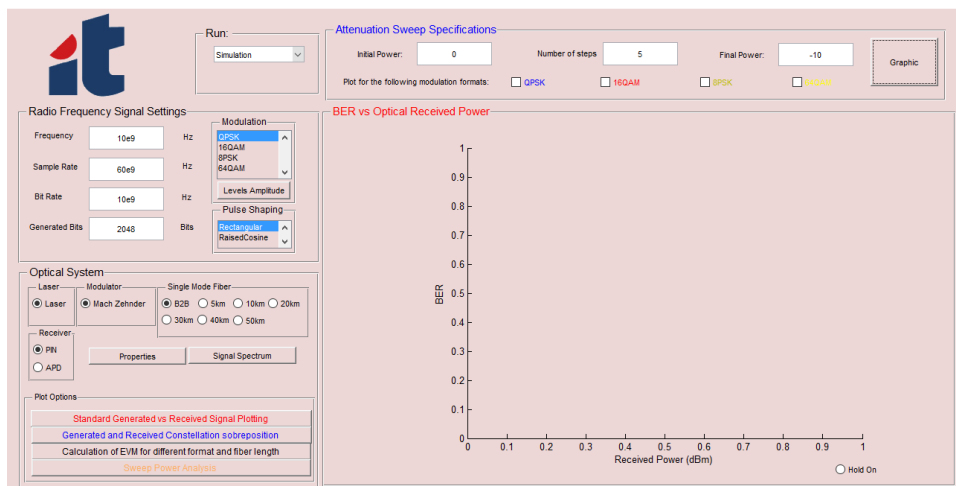

Figure A.7: Sweep Fiber Length Window

A.1.6 Results

After performing any simulation or when comparing the generated/received signals from the laboratory experiments, a window pops up indicating the results metric that have been mentioned previously. In the following figure it's possible to visualize the results obtained for a simulation performed on the simulator, and the respective results shown,
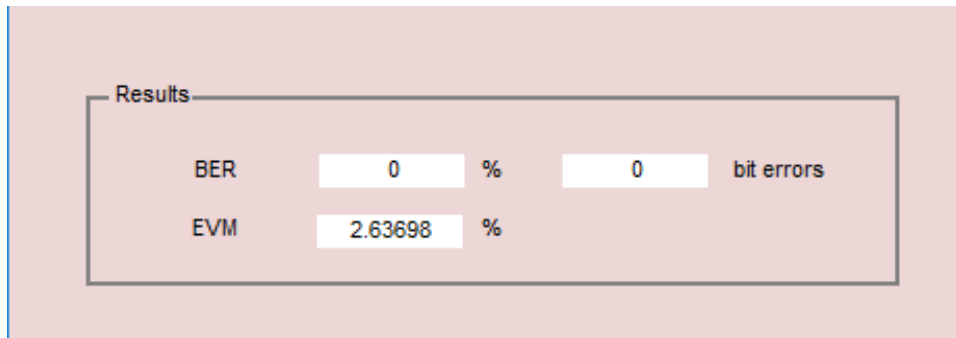
Figure A.8: Metrics results window